SEMIANNUAL TECHNICAL REPORT

1 JAN 94 to 30 JUN 94

The In Situ Observation of Epitaxial Diamond Thin Film Nucleation and Growth Using Emission Electron Microscopy

Submitted by

Martin E. Kordesch
Associate Professor of Physics
Ohio University, Athens, Ohio
Tel.: (614) 593 - 1703, FAX: - 0433
electronic mail: kordesch@helios.phy.ohiou.edu

Grant No. N00014-91-J-1596
R&T Number: s400028ssr02

REPORT DOCUMENTATION PAGE

FORM APPROVED
OMB No. 0704-0188

1. AGENCY USE ONLY (Leave blank)	2. REPORT DATE	3. REPORT TYPE AND DATES COVERED
	2-Jan-95	Semiannual 1-JAN-94 to 30-JUN-94

4. TITLE AND SUBTITLE OF REPORT
The in situ Observation of Epitaxial Diamond Thin Film Nucleation and Growth using Emission Microscopy

5. FUNDING NUMBERS
G: N00014-91-J-1596

6. AUTHOR(S)
Martin E. Kordesch

7. PERFORMING ORGANIZATION NAME(S) AND ADDRESS(ES)
Department of Physics
Ohio UNiversity
Athens, OH 45701-2979
Claire Carlson, Administrative contact

8. PERFORMING ORGANIZATION REPORT NUMBER:

9. SPONSORING/MONITORING AGENCY NAME(S) AND ADDRESS(ES)
Max N. Yoder
Office of Naval Research, ONR-312
800 N. Quincy St.
Arlington, VA 22217-5660

10. SPONSORING/MONITORING AGENCY REPORT NUMBER:

11. SUPPLEMENTARY NOTES:

12a. DISTRIBUTION AVAILABILITY STATEMENT
Approved for Public release, distribution unlimited

12b. DISTRIBUTION CODE

13. ABSTRACT (Maximum 200 words)

A variety of natural and chemical vapor deposited diamond surfaces have been imaged using a photoelectron emission microscope and synchrotron radiation in the 4-18 eV and 250-350 eV range. Both images and spatially resolved total electron yield curves were acquired simultaneously. Near-edge spectra at the carbon 1s edge show a resonance due to graphite; the image intensity varies uniformly in proportion to the C 1s edge intensity. In the 4-18 eV range, no sharp features related to a photoemission threshold were observed below 7 eV in the electron yield curves on any of the specimens. The image contrast was not strongly dependant on the illumination energy. Natural type IIa diamond showed severe charging effects.

14. SUBJECT TERMS
diamond, synchrotron radiation, near edge spectra photoemission, photoelectron microscopy, photoyield

15. NUMBER OF PAGES: 73

16. PRICE CODE

17. SECURITY CLASSIFICATION OF REPORT:	18. SECURITY CLASSIFICATION OF THIS PAGE	19. SECURITY CLASSIFICATION OF ABSTRACT	20. LIMITATION OF ABSTRACT
unclassified	unclassified	unclassified	UL

CONTENTS

page

1.0 Summary of Progress

1.1 Diamond Epitaxial Growth on Mo(310) and Si(310)

The stabilization of carbon monolayers on molybdenum surfaces at temperatures used for diamond growth by sulfur has been detailed in both a doctoral Dissertation (see Abstract appended) and in a paper submitted to J.Vac.Sci.Technol.. The details are contained in the appended preprint.

Am attempt to simulate sulfur diffusion out of the Mo(310) surface using hydrogen sulfide was unsuccessful. The stabilization mechanism is therefore most likely dynamic. The implications for diamond nucleation and epitaxy may be pervasive, if, for example, sulfur stabilization is the reason for the high nucleation rate of diamond on Mo, where sulfur is always present, and segregates to the surface during diamond growth.

1.2 Synchrotron Radiation Studies of Diamond

During January 1993, an attempt to find a negative electron affinity (NEA) signature in photoemission from diamond was made at the Wisconson Synchrotron Center in Stoughton, Wisc. PEEM images were recorded simultaneously with electron yield spectra over the 4 to 18 eV incident photon energy range. The PEEM/VUV-yield spectra would be ideal for the detection of emission sites on NEA surfaces, since the photon energy could be scanned through the emission threshold while extracting electrons from the surface using the accelerating field of the microscope objective. Results are given in the appended paper submitted to J. Vac. Sci. Technol. This work was also supported by a NATO grant.

1.3 LEEM

The LEEM was rebuilt in the early 1994 to allow independent tilt of the specimen in two mutually perpendicular axes. The sample mount was made on two large rings (150mm) connected as gimbals. The mount was made at Ohio University, since commercial manipulators (between $ 25-30,000) could not fill the need for up to 20 degrees tilt and high voltage insulation. The manipulator has been tested, and is fully functional.

1.4 Molecular Beam Deposition

The Skimmer and nozzle development on the molecular beam system were carried out in this period. Tests with 1% Argon in hydrogen were undertaken, but no conclusive results are available, since some questions about the alignment of the skimmer to nozzle accuracy remain. In the one test so far, no kinetic emission was observed with either 1% methane in hydrogen or 1% Argon in hydrogen. A simpler design, with greatly reduced skimmer to surface distances is now in the construction phase.

Investigation of Iodomethane and similar compounds was

suspended due to their toxicity. Their investigation will be postponed until proper safety measures can be instituted.

No capital equipment was purchased for the molecular beam system due to a projected shortage of funds. The pulsed nozzle and fast ion gauge purchases will be made at a later date.

1.5 Thermal Emission Microscopy of molten Cu

An undergraduate project to observe the segregation of carbon to the surface in molten Cu was completed. The observation of molten copper was not practical, since evaporation of the metal proceeded at a very high rate during observation. Manganese was choosen as a substitute, and excellent images of a dynamic melting and evaporation process, with distinct boundaries at the propogation front were observed. A short discussion is contained in the invited paper included in the appendix and submitted to J.Vac.Sci.Technol.; the thesis title page is also appended.

2.0 Publications/Presentations

Papers Published:

1. C. Wang, J.Macaulay, J.D. Shovlin and M.E. Kordesch, "An In Situ Observation of CVD Diamond Etching and Dissolution Using Photoelectron Emission Microscopy", Diamond and Related Materials, 3 (1994) 1066-71.

2. W.Engel, D.C. Ingram, J. Keay and M.E. Kordesch, "Removal of Non-Diamond Carbon from CVD Diamond Surfaces", Diamond and Related Materials, 3 (1994) 1227-1229.

3. J.D. Shovlin and M.E. Kordesch, "Electron emission from a chemical vapor deposited diamond and dielectric breakdown", Applied Physics Letters 65 (1994) 863-865.

Papers Presented at Meetings:

1. In situ photoelectron emission microscopy of oxidation and reduction of Mo(100) and Mo(310) at 1000 K, Adrian Garcia and M.E. Kordesch, APS March Meeting, Pittsburgh, March 1994. Bul. Amer. Phys. Soc. 39 (1994) 653.

2. Emission Microscopy of Low Field Cold Electron Emission from CVD Diamond Films, J.D. Shovlin and M.E. Kordesch, APS March Meeting, Pittsburgh, March 1994. Bul Amer. Phys. Soc. 39 (1994) 161.

3. Invited Lecture: Seeded Molecular Beam Growth of Diamond Observed with Emission Microscopy, Gordon Research Conference: "Diamond Synthesis", Plymouth, NH, June 1994

Program # : SS-MoP1
Put on JVST manuscript

Surface Reaction-Diffusion Fronts Observed with Photoelectron Emission Microscopy During Carbon Deposition on Mo(310)

Adrian Garcia[1] and Martin E. Kordesch
Department of Physics and the
Condensed Matter and Surface Sciences Program
Ohio University, Athens, OH 45701

ABSTRACT

In situ, real-time photoelectron emission microscopy and post-deposition scanning Auger microscopy of carbon deposition on oxygen-covered Mo(310) at 950 K shows that sulfur stabilizes the carbon layer on the Mo surface. Reaction diffusion fronts are observed to travel across the Mo surface. The leading edges of these fronts are divided into discrete bands. A model for the development of the bands based on the diffusion of carbon and sulfur and possibly other reactants is presented.

[1]Universidad Autonoma de San Luis Potosi
IICO
Alvaro Obregon # 64
78000 San Luis Potosi, SLP
Mexico

Introduction

Several in situ studies of reaction diffusion fronts have been made with Photoelectron Emission Microscopy (PEEM). Most have concentrated on the CO oxidation reaction on Pt [1-10]; some have directly addressed diffusion of adsorbates [11-13]. The PEEM is useful for diffusion studies because single monolayers are made "visible", in the PEEM image, due to the alteration of the surface work function by the diffusing adsorbate. Changes in the surface work function directly affect image contrast, since the electron yield is dependent on the relative values of the photon illumination energy and the work function. When the work function is less than the incident photon energy, electrons are emitted and the surface appears "light", the surface is "dark" in the image when the incident photon is unable to cause a photoemission event, i.e. the work function is above the illumination energy.

In an earlier study [14], the progress of two-dimensional reaction fronts of carbon deposited on oxygen covered Mo(100) was examined by PEEM alone. In this study, a "hot filament doser" similar to those used for diamond chemical vapor deposition was used [15]. The Mo(100) surface was exposed to a mixture of 5% CH_4 in hydrogen passed through a capillary and over a 2300 K tungsten filament, with the surface held at 1300 K. It was found that the deposition of carbon occurred inhomogeneously. The carbon could only be deposited in areas where the oxygen layer had been removed, presumably through a chemical reaction, since

the desorption temperature of oxygen on Mo(100) was not reached in the deposition process [16]. At the boundary between the oxygen and carbon covered surface, a "bright" band with a high photoelectron yield relative to the carbon-covered side, was observed, in situ, during deposition. The band was not present when the Mo(100) surface was cooled from the reaction temperature to less than 700 K.

The preparation of a two-dimensional carbon layer on the Mo(100) surface became more difficult with each successive attempt. Nucleation was not enhanced by purposely scratching, sputtering or otherwise mechanically abusing the Mo(100) surface. A chemical promoter of the two-dimensional growth front was suspected. This paper presents data on a new Mo(310) crystal using scanning Auger Spectroscopy that may identify the "catalyst" for two-dimensional growth, and also shows new phenomena at the boundary of the growth front that is apparent in the PEEM images as individual bands or rings in the progressing reaction diffusion front.

Experimental

The PEEM and experimental chamber have been described in refs. 17 and 18. The scanning Auger microscope (SAM) apparatus, using a VG CLAM 2 and an LEG 61 electron gun with a 3 μm spot size were added to the system on a separate chamber. The angles between spectrometer and electron gun with sample normal are 26° and 27°, respectively.

Using the transfer system described in ref. 18, the sample could be transferred from the PEEM chamber to the SAM chamber for post-deposition Auger (AES) and SAM analysis. Heating by electron bombardment was possible in both positions.

The Mo(310) crystal was cleaned by Ar-ion bombardment and repeated annealing in oxygen and subsequent flash desorption to 1700K, and several days of annealing in UHV at 1100-1300 K. Sharp 1x1 LEED patterns were observed. After the cleaning procedure, only trace carbon contamination was detected in AES.

The illumination source in PEEM is an HBO 100 mercury short arc lamp with a maximum useful photon energy of 5.1 eV

Results

PEEM micrographs of the Mo(310) surface at 950 K during exposure to the 5% methane-hydrogen mixture at 2 x 10^{-6} Torr, with the hot filament at 2300 K are shown in figure 1. Figures 1 (b) and 1 (c) were acquired at intervals of 1860 and 3040 seconds after 1 (a). The light portions (fronts) advanced at a rate of 0.03 µm/sec. The light portions in the upper half of the micrograph are low work function, high photoelectron yield areas. The dark areas correspond to a high work function, low or zero-photoelectron yield surface. The two areas are divided by a "bright band", of relatively high photoelectron yield (no thermal emission was observed in any of the experiments reported here). The small light dot in figure 1 (a), at the lower right of the field of view, is an impurity that served as a nucleation center.

The broad front at the top of the micrographs presumably nucleated at the edge of the crystal. The motion of the reaction front can be seen in the micrographs by observing the enlargement of the disk and rings around the impurity center, and by the envelopment of the cigar-like feature in figure 1 (b) that lay just ahead of the front on the dark side of the boundary in figure 1 (a). To better show the fine structure in the rings, a negative image of figure 1 (c) is shown in figure 1 (d). The leading edge of the fronts is less sharply defined relative to the dark and light bands immediately behind the boundary of the front.

Post reaction analysis showed a strong peak at 147 eV, attributed to the LVV sulfur Auger transition. A scanning Auger sulfur image (figure 2 (a)) and point Auger spectra taken <u>after</u> deposition on both sides and at the boundary (figure 2 (b)) are shown in figure 2. The position of the boundary was determined from the coordinates of the front observed in PEEM. The AES spectra and SAM clearly indicate the presence of sulfur and carbon on what was the "bright" side of the boundary. AES spectra on the "dark" portion indicate the presence of mostly oxygen, with the presence of some co-adsorbed CO inferred from the C peak lineshape. The gradual transition from oxygen covered to sulfur-carbon covered surfaces is also reflected in the gradual transition from bright to dark in the PEEM micrographs of the leading edge of the reaction front.

Larger area SAM images (~ 10mm) showed an exact

correspondence of the light and dark areas observed in PEEM and the distribution of sulphur and carbon (light) and oxygen (dark) over the entire surface.

Discussion

The scanning Auger maps confirmed the initial findings reported for the Mo(100) surface [14]. Carbon deposited on the surface corresponds to exactly to the "light" areas, oxygen covered areas are dark in the PEEM image. The SAM images, which are acquired at 300K, show that the distribution of these elements remains constant, i.e. the boundary is stable when cooled below the reaction temperature (~850 K). PEEM images show that the bright band is not present below 700 K, as reported in [14].

The presence of sulphur on the carbon side of the boundary may explain why the reaction was not observed on a Mo single crystal that was repeatedly cleaned for over one year-- the depletion of S in the crystal removed the material responsible for the stability of the carbon/sulphur phase at high temperature. A pure carbon layer would be expected to dissolve into the Mo bulk when heated.

Since no spontaneous nucleation of the carbon/sulphur layer in the oxygen layer was ever observed, the oxygen layer is clearly unreactive, impervious to attack both from the S in the bulk and from the carbon in the gas phase, except at impurity sites and at its edges. There is no sulfur source in our system

other than the Mo bulk. The oxygen layer therefore prevents sulfur segregation to the Mo surface. Growth of the carbon sulfur layer must occur at sites where both are present, and oxygen has been removed by a competing or facilitating reaction.

The indication from the AES spectra that CO can co-adsorb on the oxygen side suggests a model for progression of the reaction front, which is shown in figure 3 (a) and (b). The simple reaction front, as observed on Mo(100) [14] and on Mo(310) as shown in figure a is represented schematically in figure 3 (a). The photoelectron yield is related to the composition of the light, dark and "bright band" portions of the reaction front. The temperature where the reaction is activated, and the bright band is observed to progress across the crystal surface coincides with the desorption temperature of recombinant CO [21] or -CO (three states with T_{des} = 900, 1024 and 1240 K). The presence of carbon and oxygen in close proximity at the boundary would facilitate the desorption of oxygen as CO, while some CO would remain at the carbon oxygen boundary to react with sulfur and form the S-C film. A secondary reaction to remove oxygen from the CO in favor of a CS compound must then take place. In figure 3 (b) we suggest that reactions involving hydrogen from the hot filament doser are likely candidates, since direct reaction of sulfur and oxygen would not tent to add to the CS layer.

Figure 3 (b) also shows the CO molecule in an unusual bonding arrangement [22], which serves to reinforce the idea that the CO in the "bright band" is in an electronic state that is not

similar to chemisorbed CO on Mo, since the "bright band" implies a photoelectron yield far in excess of that observed for adsorbed CO. The reaction between S and the CO in the band may also be responsible for a high photoelectron yield precursor, but there is no independent measurement to prefer such an interpretation.

The multi-banded reaction front is schematically shown in figure 4 a, a reaction model is shown in figure 4 (b). Since our SAM does not sufficiently resolve the individual bands, and the PEEM image cannot distinguish two different adsorbates with similar work function, some speculation is necessary for the interpretation of the multi-banded structure. Banding in chemical reactions due to reactant precipitation (no stirring, no convection) is known from colloid chemistry and mineralogy, and the bands are termed Liesegang rings [23, see also 1-6]. In a simple view of these reactions, two reactants interdiffuse at a boundary, with a non-soluble, immobile reaction product that precipitates when a specific concentration of the reactants is reached. The depletion of the adjacent areas causes the "space" between the rings. When the critical concentration is again reached, another ring deposits.

The multi-banded reaction front is similar to the Liesegang reaction due to the probable involvement of several species with different diffusion characteristics. The advance of the front, designated W, is due to the same mechanism (-CO desorption) as the bright band in figure 3. The soft leading edge of region W (observed in PEEM, see fig. 1 (c),(d)) reflects the slow

progression of the front, 0.03 μm/s on Mo(310) compared with 2 μm/s for the singly banded front on Mo(100) [14,20]. The slow progress of the front allows reactants to diffuse past region W to the regions X,Y and Z, where we speculate that the different penetration rates for carbon and hydrogen allow sulfur removal in region Y behind a precursor carbon-sulfur film in region X. In this scheme, Y and W are assumed to be chemically similar regions, as are X and Z.

An Auger line scan through one of the multi-banded disks failed to reveal the ring structure. In fact, if regions X and Z are similar in chemical composition they would not be resolved in SAM, as opposed to PEEM.

A difficulty with the Liesegang model is the fact that there is a single set of rings, and they move along with the front. The SC film either ages, with an ensuing decrease in the photoelectron yield after the reaction, or a section of the film, X, must be removed and redeposited at Z. There does not seem to be a stationary precipitate phase.

Summary

PEEM images and SAM images of two dimensional reaction diffusion fronts on the Mo(310) surface at 950 K show that the deposition of carbon as a continuous layer is stabilized by sulfur diffusing from the bulk. The concentration of chemisorbed oxygen on the surface controls the deposition of the sulfur-carbon layer by preventing sulfur segregation from the bulk and

carbon adsorption from the gas phase. In situ PEEM observations show that several reaction intermediates are present at the reaction boundary, and these reaction products are separated into discrete bands. The multi-banded structure of the reaction interface is attributed to differing diffusion rates and mobility of the reactants on the Mo(310) surface at 950 K.

Acknowledgements

This work was supported by the Ballistic Missile Defense Organization Office of Innovative Science and Technology through Grant No. N 00014-J-91-1596.

References:

{garcia,kordesch}@helios.phy.ohiou.edu

1. V. Gorodetskii, J. Lauterbach, H.H. Rotermund, J.H. Block and G. Ertl, Nature (1994) 370; 276.

2. M. D. Graham, I. G. Kevrekidis, A. Asakura, J. Lauterbach, K. Krischer, H.H. Rotermund and G. Ertl, Science (1994) 264, 78.

3. H.H. Rotermund, Surf.Sci. (1993) 283, 87.

4. G. Veser, F. Mertens, A.S. Mikhailov and R. Imbihl, Phys.Rev. Lett. (1993) 71, 935.

5. G. Ertl, Science (1991) 254, 1750.

6. S. Jakubith, H.H. Rotermund, W. Engel, A. von Oertzen and G. Ertl, Phys. Rev. Lett. (1990) 65, 3013.

7. B. Rausenberger, W. Swiech, W. Engel, A.M. Bradshaw and E. Zeitler, Surf. Sci.(1993) 287/288, 235.

8. B. Rausenberger, W. Swiech, C.S. Rastomjee, M. Mundschau, W.Engel, A.M. Bradshaw and E. Zeitler, Chem.Phys.Lett. 125, 109 (1993).

9. M.E. Kordesch, W. Engel, E. Zeitler and A.M. Bradshaw, J. Phys.: Cond. Matter, 1, SB1-SB6 (1989).

10. M. Mundschau, M.E. Kordesch, W.Engel, B. Rausenberger, E. Zeitler and A.M. Bradshaw, Surface Science, 227 (1990) 246.

11. M. Ondrejecek, W. Stenzel, H. Conrad, V. Chab, Z. Chvoj, W. Engel and A.M. Bradshaw, Chem. Phys. Lett. 215, 528 (1993).

12. A. Van Oertzen, H.H. Rotermund and S. Nettesheim, Chem Phys.

Lett. 199, 131 (19920.

13. H.H. Rotermund, S. Nettesheim, A.Von Oertzen and G. Ertl, Surf. Sci. Lett. 275, L645 (1992).

14. A. Garcia. C. Wang and M.E. Kordesch, Appl. Phys. Lett. 61, 2984 (1992).

15. F.G. Celii and J.E. Butler, Annu. Rev. Phys. Chem.,42, 643 (1991).

16. E. Bauer and H. Poppa, Surf. Sci. 88, 31 (1979).

17. W. Engel, M.E. Kordesch, H.H. Rotermund, S. Kubala and A. van Oertzen, Ultramicroscopy **36**,148 (1991).

18. C. Wang and M. E. Kordesch, Ultramicroscopy **36**, 154 (1991).

19. A. Garcia and M. E. Kordesch, J. Vac. Sci. Technol., A11, 461 (1993).

20. A. Garcia, Ph.D. Dissertation, Ohio University, 1994.

21. E.I. Ko and R.J. Madix, Surf. Sci. 109, 221 (1981).

22. S.R. Morrison, The Chemical Physics of Surfaces, Plenum Press, New York, 1990, pg 205.

23. D.A. Smith, J.Chem. Phys.81, 3102 (1984), and D.S. Chernavskii, A.A. Polezhaev and S.C. Mueller, Physica D 54, 60 (1991).

Figure Captions:

Figure 1.- (a) Island growth around a nucleation center (bottom) and growth in a front-like fashion (upper left). The front advances in the direction of the arrows. A bright band forms around both the cigar-shaped feature and along the boundary separating regions of high and low work function. (b) From the first growth stages, an annular structure around the nucleation center develops. Micrographs (a), (b), and (c) were taken at t = 0, 31, and 84 min, respectively. (d) To enhance the structure developed in the reaction area, and around the nucleation center, the negative of micrograph (c) is presented. The field of view is 260 μm.

Figure 2.- (a) Sulfur image of a portion of the boundary, at 80X magnification (2500 eV, 2 mA). The image is normalized so that the brightness of the image is proportional to the abundance of sulfur. (b) Point Auger analysis was performed at the positions indicated by the X marks in (a). Besides the S $L_{23}M_{23}M_{23}$ (147 eV), the Mo $M_{45}N_1N_{23}$ (118 eV), $M_{45}N_{23}V$ (183 eV), $M_{45}VV$ (218 eV) Auger transitions are identified, as well as the O KLL (510 eV) and C KVV (266 eV) transitions. Going from X1 to X3, one can observe a decrease in the S $L_{23}M_{23}M_{23}$ Auger transition, and, simultaneously, an increase in the O KLL transition.

Figure 3.- (a) Schematic of the bright area observed in PEEM. A side view of the surface (top) showing the reaction area formed between the deposited sulfur--carbon film on the left (SC-side), and the oxygen film on the right (O-side). The graph at the bottom represents the spatial variation of the photoelectron yield of the surface. (b) Model of the front traveling toward the O-side. At the desorption temperature (~900 K), atomic C and O recombine on the surface and desorb as molecular CO. Then, H_2 and CO dissociatevely adsorb removing oxygen and sulfur as H_2O and H_2S , respectively. Oxygen is removed at the leading edge of the reaction area, and the front advances toward the oxygen film.

Figure 4.- Schematic representation of the multi--band structure. The reaction area observed during deposition with the substrate at 950 K showed four bands. The band next to the oxygen film is bright (W). The width of this band increased during deposition. Behind the first band came two thinner bands. The first one is dark (X), and the second one bright (Y). The width of these two bands remained constant throughout the observations. The width of the fourth band (Z) also increased during deposition, in the same direction as the leading edge of band W, but at a slower rate. The relative photoelectron yield of the multiband system is shown schematically at the bottom of the figure. (b) Model of the multi-band structure observed in the reaction area. Adsorbed atomic species (H, C, and O) diffuse

from the reaction area towards the growing sulfur-carbon film. The multi-band structure is formed due to concentration gradients created by surface diffusion of hydrogen, carbon, and oxygen atoms competing for surface sites against sulfur segregation from the bulk.

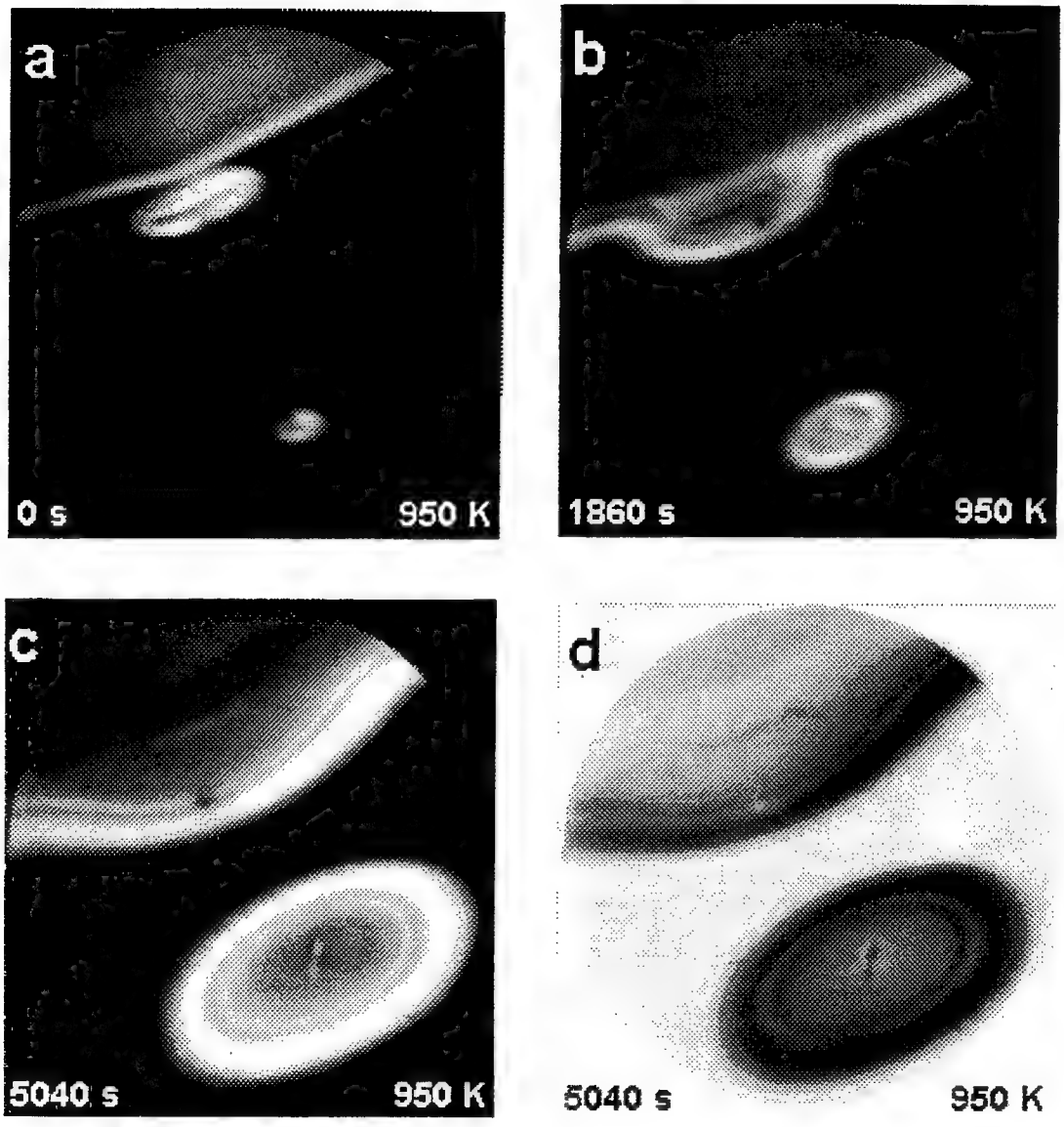
a
0 s
950 K
b
1860 s
950 K
c
5040 s
950 K
d
5040 s
950 K

a

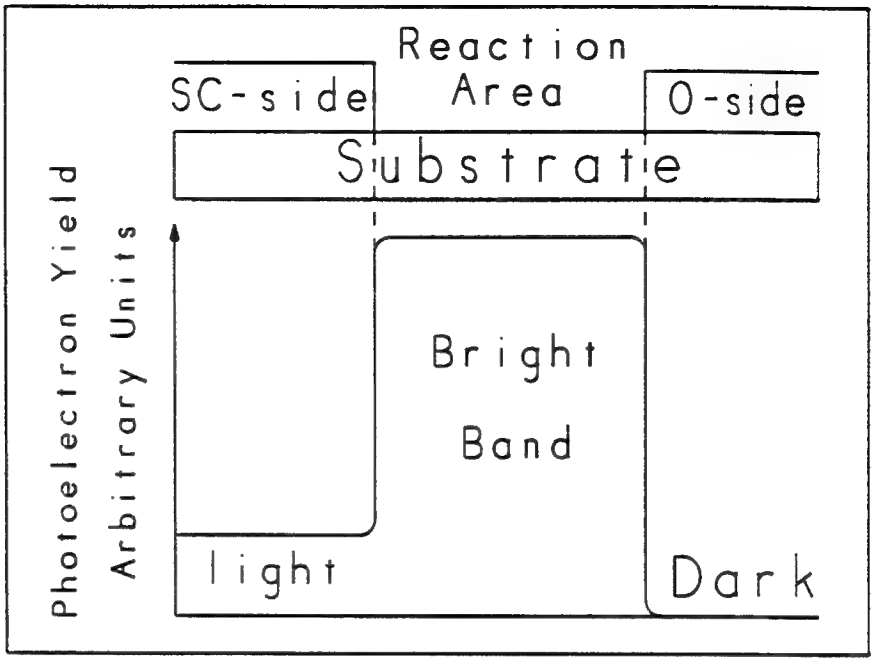
Reaction
Area
SC-side
O-side
Substrate
Photoelectron Yield
Arbitrary Units
Bright
Band
light
Dark

b

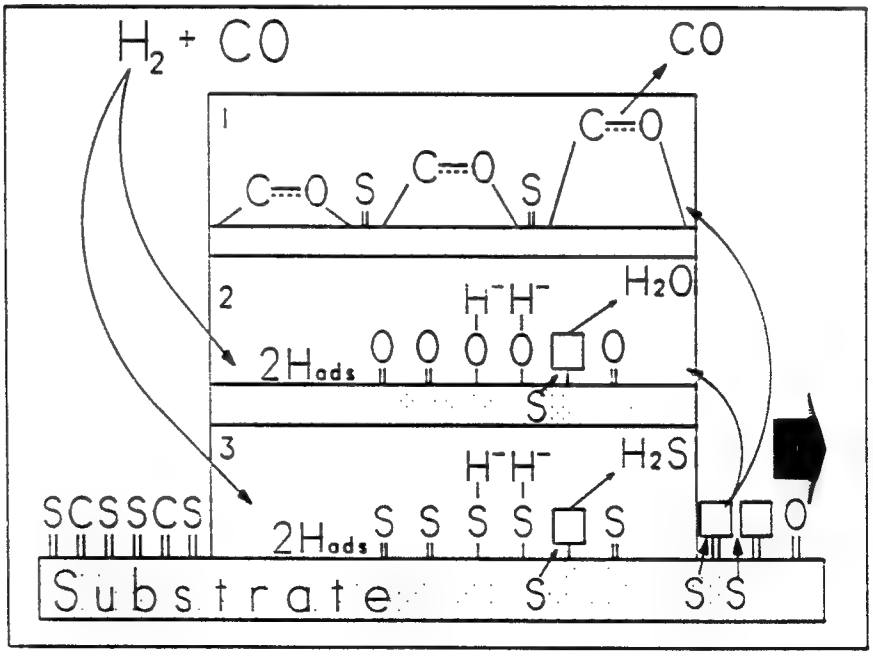
H2 + CO
CO
1
C=O
S
2
H2O
2Hads
3
H2S
SCSSCS
Substrate

a

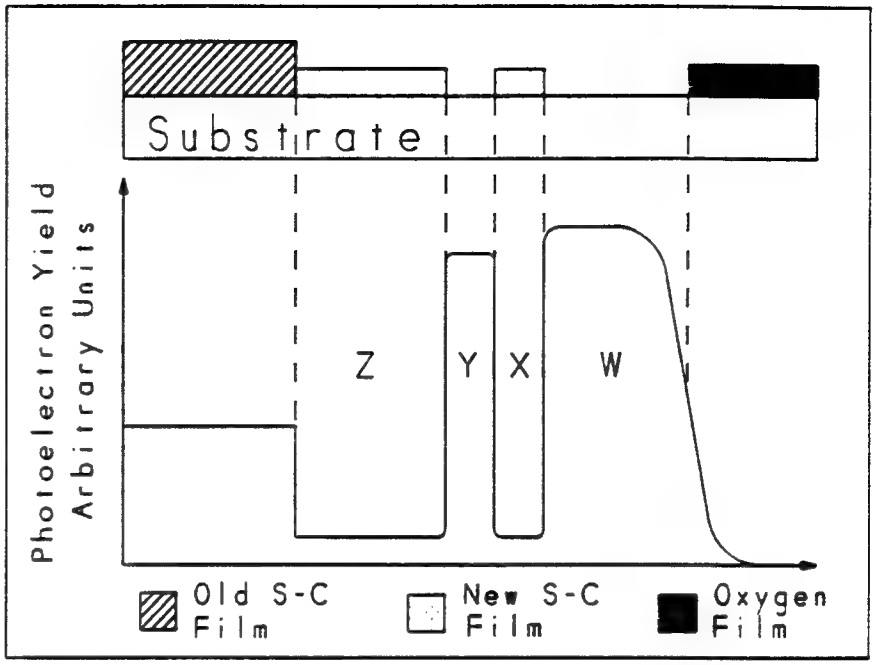
Substrate
Photoelectron Yield
Arbitrary Units
Z
Y
X
W
Old S-C Film
New S-C Film
Oxygen Film

b

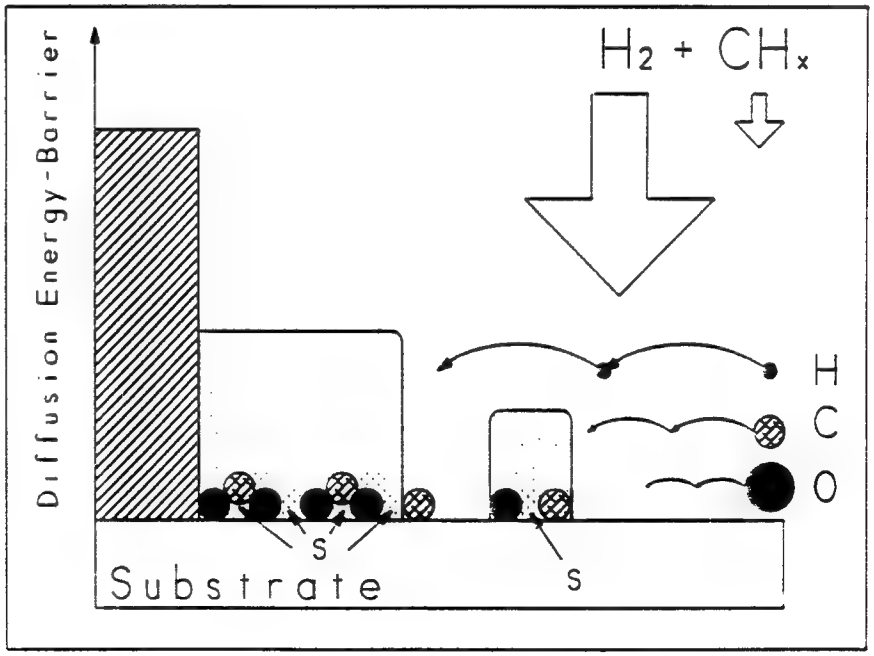
Diffusion Energy-Barrier
H2 + CHx
H
C
O
S
S
Substrate

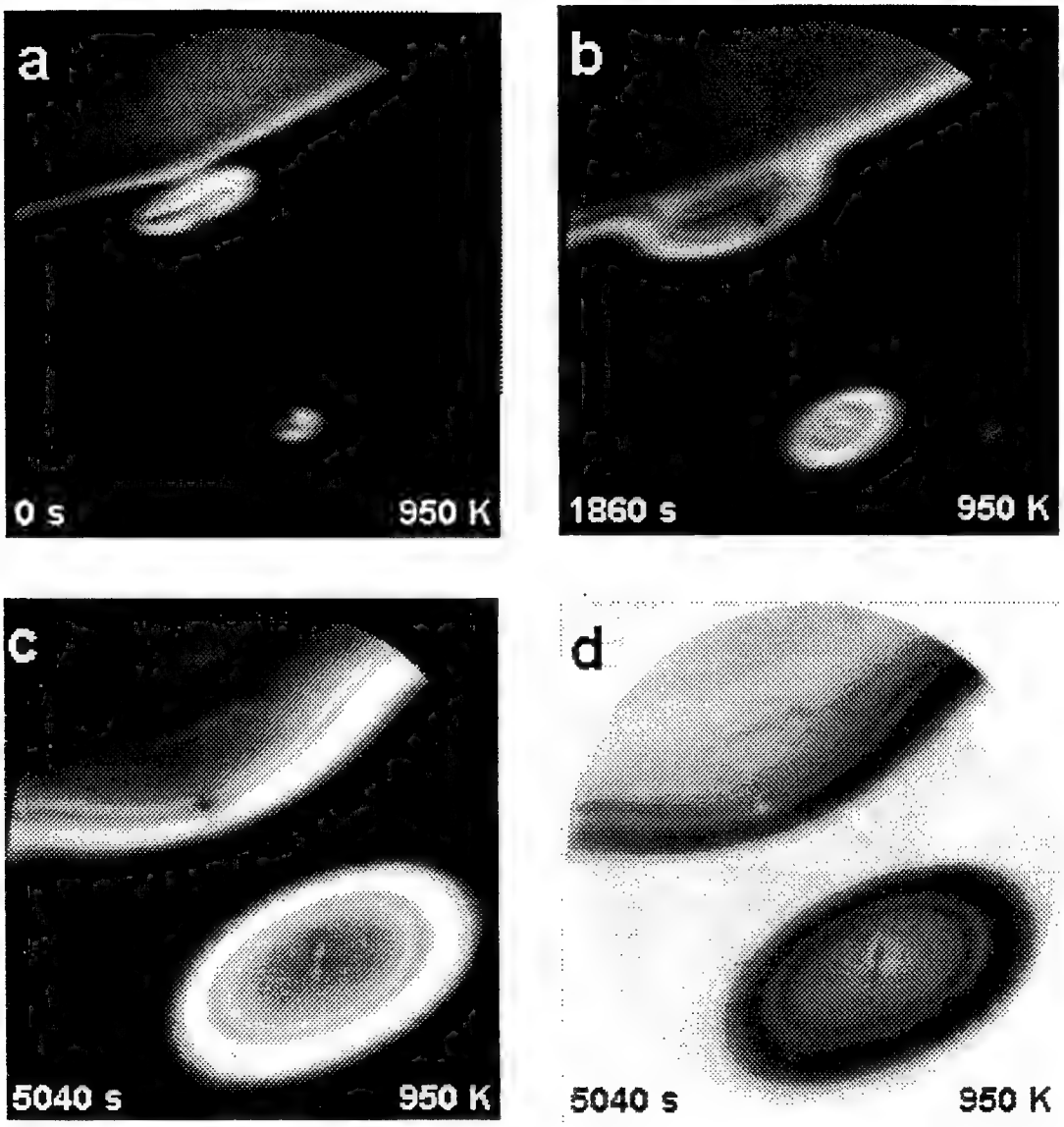
a
0 s
950 K
b
1860 s
950 K
c
5040 s
950 K
d
5040 s
950 K

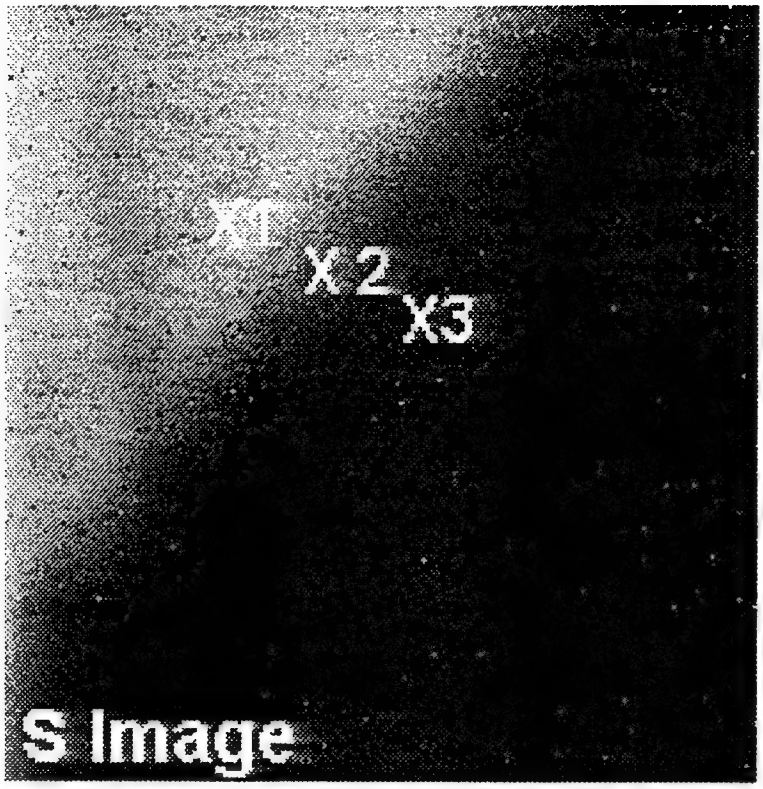
X1
X2
X3
S Image

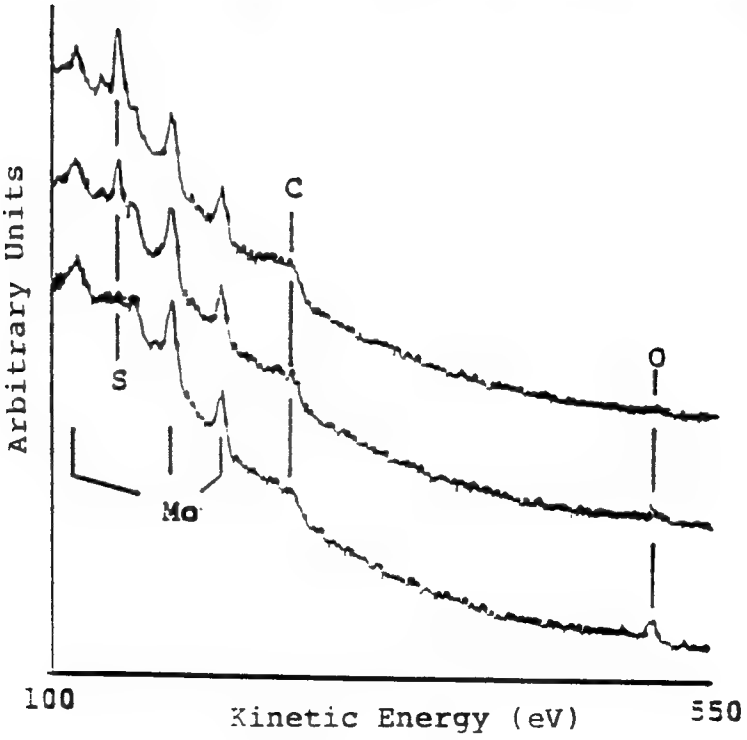
Arbitrary Units
C
S
O
Mo
100
Kinetic Energy (eV)
550

Abstract # : 31
Program # : SS1-TuA5
INVI
Put on JVST manuscript

Probing Reactive Deposition and Surface Dynamics Using In Situ, Real-Time Emission Microscopy

Martin E. Kordesch
Department of Physics and the
Condensed Matter and Surface Sciences Program
Ohio University, Athens, OH 45701

ABSTRACT

Emission Microscopy images of surface processes during chemical vapor deposition and catalytic reactions show a number of dynamic reaction phenomena that illustrate problems suitable for observation with the emission microscope: nucleation and growth of adsorbed layers, adsorbate controlled diffusion from the bulk, pattern formation, melting and evaporation. A qualitative examination of deposit morphology and are compared to the formation of Liesegang rings.

Introduction

Emission microscopes have flourished at various times in the past 60 years, only to be eclipsed by the transmission and scanning electron microscopes. The advent of the Bauer-Telieps "Low Energy Electron Microscope" (LEEM) [1] in the 1980's has brought about another "emission era" [1-32].

Some of the most striking emission microscopy images of surface reactions are from observations of the catalytic reaction of CO and oxygen on Pt surfaces [2-11]. The first emission microscope experiments on the CO-Pt system date back to the 1930's when Pohl [12] compared thermionic and photoelectric emission from Pt foils. There is a large body of literature that has provided data to simulate and model the dynamics of the CO oxidation reaction on Pt and other metals. In comparison with the CO-Pt system, studies of other systems have just begun.

One of the most pervasive "types" of deposition phenomenon observed with the emission microscope is nucleation of a deposit at an impurity or defect, and subsequent progression of the reaction as a front, or band (rings), sometimes with a reaction region at the leading edge of the front with enhanced electron emission. The formation of a reactive band at the leading edge of the reaction is reasonable, since the boundary atoms are more exposed to reaction than those in the interior. In practice, however, the shape and structure of the leading edge may be extremely complex. In this paper, examples of submono- to multi-layer deposition at elevated temperature (350 - 1500 K) in a

reactive environment will be shown, with emphasis on "banding", and inhomogeneous nucleation and growth of the deposit.

Experimental

In a thermal (or thermionic) emission microscope, the electron yield from a surface as a function of temperature produces image contrast. In the photoelectron emission microscope (PEEM), variations in photoelectron yield is the main source of contrast and image intensity. For a given illumination energy, if the surface has a work function less than the illumination energy, some photoelectrons will be ejected to form an image. When the work function is greater than the illumination energy, there will be no photo-electron emission, and hence no intensity in the image. In our experiments, the illumination energy of the Hg arc lamp is about 5.1 eV, so that the oxygen covered molybdenum surface is totally dark in the image, but the carbon covered surface is bright. For Pt, a deuterium lamp is used, with a cutoff energy of 6.9 eV. By using this difference in electron yield to differentiate between oxygen and carbon covered areas of the surface, the growth of the carbon overlayer may be observed in situ, in real-time.

The images presented below were acquired with two types of emission microscope. One is a LEEM-type instrument based on the Bauer-Telieps original [27]. The Ohio University LEEM uses an electrostatic objective lens designed by G.F. Rempfer [28]. The other type are small, flange-on electrostatic microscopes [29].

The design of the latter type is also based on lens data by Rempfer. The thermal emission microscope uses an objective lens adapted from the LEEM.

The specific conditions for the acquisition of each of the micro graphs is given below. The specimen holder has been described in ref.[30]. In each case, an electric field of ~50 kV/cm is applied between the specimen and the microscope objective lens.

Results:

A simple example [26] of a reaction-diffusion front is given in figure 1. The image was acquired using a deuterium lamp, on CO covered Pt(100) at 350 K. In the image, a microdust particle serves as a nucleation center for oxygen adsorption. The particle allows reaction of the adsorbed CO layer around the particle with adsorbed oxygen. At the boundary, CO_2 is produced, which desorbs. The area behind the advancing boundary is filled with adsorbed oxygen. In this example, the reaction nucleates on an impurity and travels away from the nucleation site while the adsorbed layer is removed and replaced with another reactant. The field of view is 100 μm.

In figure 2, the thermal desorption of powdered Mn dusted onto a polycrystalline Mo substrate [31] is shown in thermionic emission microscopy, at about 1500 K. Only a thin band of actively desorbing Mn is observed, the Mn film and the Mo substrate have electron yields substantially less than the

reactive band. In this example, the desorption reaction nucleated at the edge of the substrate, and the reaction front moved inward to the center of the specimen, until the reaction ceased upon total desorption of Mn. The field of view in the micrograph is 2mm.

Figures 3 and 4 are micrographs taken after carbon deposition on oxygen covered Mo(100) at 1000 K, from a 5% methane in hydrogen mixture passed over a hot tungsten filament to produce atomic hydrogen [32]. In this experiment, the pressure in the chamber was ~ 10^{-4} Torr, with the gas stream directed at the surface through a doser. The center of the crystal showed disk-like carbon deposits nucleated on impurity centers (fig. 3), while the edge of the crystal showed dendritic growths that were often nucleated on impurities (fig. 4). The composition of both of these deposits is thought to be Mo-carbide. The deposits were very difficult to remove; several days of sputtering and oxygen exposure at high temperature were necessary. X-ray photoelectron spectroscopy also confirmed the presence of Mo-carbide.

Figures 5 and 6 show chemical vapor deposited carbon on Mo(100) (1300 K) and Mo(310) (950 K), respectively, from the same hydrogen/methane mixture used in figs. 3 and 4. The chamber pressure was in the 10^{-6} Torr range. At the growth boundary on Mo(100) (fig. 5), a bright (high electron yield) band is observed where the new growth occurs [25]. The bright region is not observed at low temperatures, and is a feature only observable in situ. On Mo(310), a double band is observed (fig.6)[32,33], with

the other characteristics similar to the Mo(100) image. Both of these deposits are easily removed with high temperature oxygen treatment. The carbon deposit on Mo(310) is known to contain some sulfur.

Discussion

From the micrographs in figures 1-6 it is apparent that several layers of complexity are involved in explaining or accounting for the structure of the deposit. The growth rate, composition, microstructure, stability, electronic properties and probably several more important parameters have been ignored or remain unknown even after the images are recorded. It should be noted that once the reaction environment is altered, i.e. the reactant flow stopped or a change in temperature is made, the entire surface and the images obtained from it may change completely. We have had limited success with post deposition analysis, and some post-deposition scanning Auger images have helped with interpretation of the images on Mo surfaces.

On a superficial level, the CO oxidation reaction (fig. 1) is the simplest of the examples, because no "bright band" or "intermediate species" is resolved in the PEEM micrograph. The reaction takes place only at the boundary between the two adsorbed species, and the reactants and products are known. The examples in figures 1-6 have been reduced to schematic form in figure 7, a)-f), figure 7a) represents the CO oxidation reaction. After the reaction starts, the adsorbed CO is consumed, and

oxygen adsorbs behind the travelling front. The adsorption is fast, and does not depend on the initial nucleation site to continue. There is no evidence in the micrograph that transport of oxygen from the original dust particle to the leading edge of the front takes place. No "trailing edge" of the front is observed. In the fastest direction, the front moves at over 6 μm/sec.

The second diagram, fig. 7 b) represents the desorption of Mn from a Mo surface at 1500 K. The removal of the film nucleates at sites near the edge of the substrate, and proceeds toward the center, until the Mn is entirely removed. There is a "bright band", a leading edge of the front that has a higher electron yield than both the original film and the substrate. Speculative explanations of this band are based on melting of the film at the boundary-- either through momentarily improved thermal contact or a "flux" effect, where an oxide coating, for example, is desorbed and allows the Mn to melt and desorb [31]. In this case, and in those discussed below, a new, intermediate phase or compound is formed at the reaction front, over a width that can be resolved on both time and length scales by emission microscopy. The evaporation front is also relatively fast, moving about 10-20 μm/sec (strongly temperature dependent!).

The deposits in figures 7 c)-f) are fundamentally different from the first two. The micrographs in figure 3 and 4 are slow processes that are results of the combined action of surface diffusion and the nucleation center: they grow by addition of

material to the boundary from the outside, in front of the leading edge (fig. 7 c) and d). The nucleation center in figure 7 a), in contrast, can be thought of as a "lightning rod" or pipeline for adsorption of oxygen from the gas phase, which is initially channeled to the surface through this center to the reaction front: growth occurs from the "inside" of the deposit.

The dendrite formation and multi-ringed disks around the nucleation centers in fig. 3 and 4, and 7 c) and d) are formed by the migration of a surface adsorbate to a pinning center, where further motion is halted. On the disk (7 c)), no specific site is necessary for adhesion by the diffusing species, the isotropic addition of material forms rings (in fig. 3, however, the centers of the deposits are squares, showing fast and slow diffusion directions on the (100) surface). In the dendrites, inclusion in the growing fingers is reduced to a few preferred sites, at the ends of the fingers, and certain side branches (note that the fingers often follow the (100) surface orientation). In these examples, the morphology of the deposit clearly indicates that a mobile, diffusing species is captured in the deposit, where it is stabilized.

These characteristics of growth by band formation and stabilization through a reaction are known from mineralogy and the formation of agates. Figure 8 shows a photograph of a slice of agate. The banding is clear in the photograph; an explanation was given by Liesegang [34], and further expanded by Ostwald [35]. The rings are named after Liesegang. In the non-

convective (stirring or convection destroys the bands) interdiffusion of two reactants, an insoluble product can precipitate when a critical concentration is reached. The precipitate is immobile, and the depletion areas on each side of the band form the empty spaces between the bands. When the critical concentrations are again reached, a new band is deposited. The details of the Liesegang phenomenon are still controversial, but even the simple version of the concept seems applicable to the bands and rings in the deposits shown in figures 3 - 6. The PEEM micrographs in figures 5 and 6 strongly suggest a precipitation-stabilization reaction related to the Liesegang ring model.

In figure 5, and 6, carbon deposited on the oxygen covered Mo(100) and (310) surfaces deposits in the form of an extended front with a bright leading edge. On Mo(310), the leading edge is divided into two bands. The schematic representation is shown in figure 7 e) and f). On the Mo(100) surface, the experimental conditions were such that the reaction front was moving at about 2 µm/sec, and the front was not observed to divide or form a double band. On Mo(310), the progress of the front was on the order of 0.01 µm/sec. The different front speeds were associated with different diffusion phenomena by post reaction Auger analysis.

Analysis of the carbon deposits on Mo(310) with scanning Auger spectroscopy showed that the light areas observed in PEEM were not pure carbon, but contained sulfur [33]. As no gas phase

source of sulfur was present, it is believed that the sulfur found in the deposits diffuses from the bulk of the Mo crystal during the deposition. Because no secondary nucleation of a sulfur-carbon deposit is ever observed on the oxygen covered Mo surface, it is also evident that oxygen suppresses sulfur segregation to the Mo surface at the deposition temperature.

Based on the Liesegang model, a possible explanation of the divided leading edge is the penetration of the reaction front by a more mobile reactant that is able to remove material from the center or trailing edge of the front. For example, if the "bright band" consists of a combination of diffusing and reacting carbon and oxygen (with CO as a desorption product) and sulfur diffusing from the bulk to the surface in the band, some sulfur can combine to form the stable S-C deposit, and some sulfur could be removed from the deposit by adsorbed hydrogen travelling through the band from the oxygen side. The very slow progress of the front in this deposition process would allow the formation of a new band. The sulfur concentration in the reaction area determines the structure of the band. In this case, the interdiffusion of the reactants results in bands due to concentration gradients at the interface, but the entire complex moves with the front rather than a deposition of stationary rings or bands.

Unfortunately, PEEM can distinguish high and low electron yield regions on a surface, but not chemical composition. We are unable to determine if the dark center ring, between the two

bright rings of the front on Mo(310) is oxygen covered, or some other type of material or compound. Post-reaction analysis with Auger spectroscopy does not resolve the bands.

In reactions where several compositional phases compete during a complex reaction, such as low pressure low temperature diamond growth; adsorption, parasitic reactions, surface and bulk diffusion, dissolution of reactants and products into the substrate and time dependant evolution of the growth surface that either promote or poison the reaction often take place. In this environment optical and electron spectroscopy are not easily accommodated, and the spatial distribution of the reactants is unknown. PEEM has made some contribution to the phenomena encountered in the early stages of diamond growth on Mo substrates [36], in particular through the identification of Mo-carbide as a diffusion barrier during the initial stages of diamond growth. Studies of diamond deposition and other non-equilibrium reactions where the reactants arrive at the surface with supra-thermal kinetic energies using in situ emission microscopy are planned.

Summary

By a qualitative discussion of several kind of carbon deposits on Mo and Pt surfaces that can be observed in situ with emission microscopy, the morphological characteristics of deposits have been linked to diffusion rates, reaction rates and defects. A qualitative explanation of rings and bands formed

during carbon deposition on Mo based on the interdiffusion of two species with subsequent precipitation of a third reaction product and the formation of Liesegang rings is proposed.

Acknowledgments:

The contributions of Adrian Garcia and Steve Pellathy in obtaining the PEEM and Thermal emission images are gratefully acknowledged. Joe Shovlin created the diagrams in figure 7 and the agate photograph. Mike Mundschau pointed out the original references to Liesegang's work. Various parts of this work were supported by the Ballistic Missile Defense Organization (BMDO) through the Office of Innovative Science and Technology grant N00014-J-91- 1596. Support from NATO and the BMDO SBIR program is also acknowledged.

References:

email:kordesch@helios.phy.ohiou.edu

1. E. Bauer, Surf.Sci. 299/300, 102 (1994).

2. V. Gorodetskii, J. Lauterbach, H.H. Rotermund, J.H. Block and G. Ertl, Nature 370, 276 (1994).

3. M. D. Graham, I. G. Kevrekidis, A. Asakura, J. Lauterbach, K. Krischer, H.H. Rotermund and G. Ertl, Science 264, 78 (1994).

4. H.H. Rotermund, Surf.Sci. 283, 87 (1993).

5. G. Veser, F. Mertens, A.S. Mikhailov and R. Imbihl, Phys.Rev. Lett. 71, 935 (1993).

6. G. Ertl, Science 254, 1750 (1991).

7. S. Jakubith, H.H. Rotermund, W. Engel, A. von Oertzen and G. Ertl, Phys. Rev. Lett. 65, 3013 (1990).

8. B. Rausenberger, In-Situ Untersuchungen heterogen-katalysierter Reaktionen an Einkristalloberflächen mit Emissions- und Reflexions- mikroskopie langsamer elektronen, Verlag Köster, Berlin, 1993.

9. B. Rausenberger, W. Swiech, W. Engel, A.M. Bradshaw and E. Zeitler, Surf. Sci. 287/288, 235 (1993).

10. W. Swiech, B. Rausenberger, W. Engel, A. M. Bradshaw and E. Zeitler, Surf. Sci. 294, 297 (1993).

11. B. Rausenberger, W. Swiech, C.S. Rastomjee, M. Mundschau, W. Engel, A.M. Bradshaw and E. Zeitler, Chem.Phys.Lett. 125, 109 (1993).

12. J. Pohl, Physik. Zeitschr. 35, 1003 (1934).

13. R. M. Tromp and M.C. Reuter, Phys.Rev.Lett. 73, 110 (1994).

14. J. Tersoff, A.W. Denier van der Gon, and R.M. Tromp, Phys.Rev.Lett. 72, 266 (1994).

15. R.M. Tromp, A.W. Denier van der Gon, F.K. LeGoues, and M.C. Reuter, Phys.Rev.Lett. 71, 3299 (1993).

16. J. Tersoff and R.M. Tromp, Phys.Rev.Lett. 70, 2782 (1993).

17. A.W. Denier van der Gon and R. M. Tromp, Phys. Rev. Lett. 69, 3519 (1992).

18. R.M. Tromp, A.W. Denier van der Gon and M.C. Reuter, Phys. Rev. Lett. 68, 2313 (1992).

19. R.M. Tromp and M.C. Reuter, Phys. Rev. Lett. 68, 954 (1992), and Phys. Rev. Lett. 68, 820 (1992).

20. R.J. Phaneuf, et al., Phys. Rev. Lett. (1991) 67, 2986.

21. H. Pinkvos, et al. Ultramicroscopy (1992) 47, 339.

22. W. Telieps, Appl. Phys. A,(1987)44, 55.

23. E. Bauer and W. Telieps, in Surface and Interface Characaterization by Electron Optical Methods, A. Howie and U. Valdre, eds. New York: Plenum Publishing Corp. 1988.

24. J. Stohr, et al. Science 259, 659 (1993).

25. A. Garcia. C. Wang and M.E. Kordesch, Appl. Phys. Lett. 61, 2984 (1992).

26. M. Mundschau, M.E. Kordesch, B. Rausenberger, W. Engel, A. M. Bradshaw and E. Zeitler, Surf. Sci 227, 246 (1990).

27. W. Telieps and E. Bauer, Ultramicroscopy 17, 57 (1985).

28. G. Rempfer, J. Appl. Phys. 57, 2385 (1985).

29. W. Engel, M.E. Kordesch, H.H. Rotermund and A.van Oertzen Ultramicroscopy 36 (1990).

30. A. Garcia and M. E. Kordesch, J. Vac. Sci. Technol., A11, 461 (1993).

31. A. Garcia, Ph.D. Dissertation, Ohio University, 1994.

32. S. Pellathy, A. Garcia and M.E. Kordesch, unpublished data.

33. A. Garcia and M.E. Kordesch, J. Vac. Sci. Technol.:submitted.

34. R.E. Liesegang, Die Achate, Dresden, 1915. Cited in The Problem of Physico-Chemical Periodicity, E.S. Hodges and J.E. Myers, Longmans, Green and Co., New York, 1926.

35. M.E. Le Van and J. Ross, J.Chem.Phys. 91, 6300 (1987).

36. C. Wang, J.D. Shovlin, M.E. Kordesch and J.M.Macaulay, Diamond Relat. Mater. 3, 1066 (1994).

Figure Captions:

Figure 1. : PEEM micrograph of the nucleation of the CO oxidation reaction front at a microdust particle at 350 K. The photographs are taken at 2 sec intervals, starting at top right. The dark disk in each frame is the field of view, 100 μm.

Figure 2. : Thermal emission micrograph of melting and evaporation of Mn dust on Mo at 1500 K. Filed of view 2 mm.

Figure 3. : PEEM micrograph of carbon deposits on Mo(100). Note the rings around the nucleation centers, and the rectangular centers of the deposits. Field of view is 100 μm.

Figure 4. : PEEM micrograph of Mo-carbide dendrites on Mo(100), field of view 100 μm. The background in this image is light because the oxygen layer has been removed in the reaction.

Figure 5. : PEEM micrograph of carbon deposition on oxygen covered Mo(100) at 1300 K, 10^{-6} Torr 5% methane in hydrogen. The dark side is oxygen covered, the light side is carbon covered. The front is moving from the top left to bottom right. Field of view is 80 μm.

Figure 6. : PEEM micrograph of carbon-sulfur deposition on oxygen covered Mo(310) at 950 K, 10^{-6} Torr 5% methane in hydrogen. Field of view 260 μm.

Figure 7. : Schematic represtation of the fronts in figs 1-6.

a) Simple reaction at a nucleation center (black dot). B-covered substrate removed by reaction with A, A covered surface results. The front moves from the nucleation center

outwards.

b) Thermal desorption of A from substrate B, nucleated at crystal edges.

c) Ring formation of material A around a nucleation center. The diffussion of A material on the substrate B enlarges the perimeter of the deposit. Discrete rings in the deposit may form due to the Liesegang process.

d) Dendrite formation of A at a nucleation center.

e) Reaction-diffusion front during deposition of A on B. The deposit forms through a reaction area represented by a band or ring at the leading edge of the front. Material is added by diffusion of A to the perimeter of the deposit and the reaction band. Liesegang rings may also form.

f) Reaction diffusion front with discrete bands in the reactive area. The multi banded structure results from penetration of the reaction band by a fast species, the growth of A is stabilized by a slow species diffusing from the bulk crystal at the reaction area. A moving Liesegang ring is formed.

Figure 8. : Photograph of an agate. Diameter 75 mm.

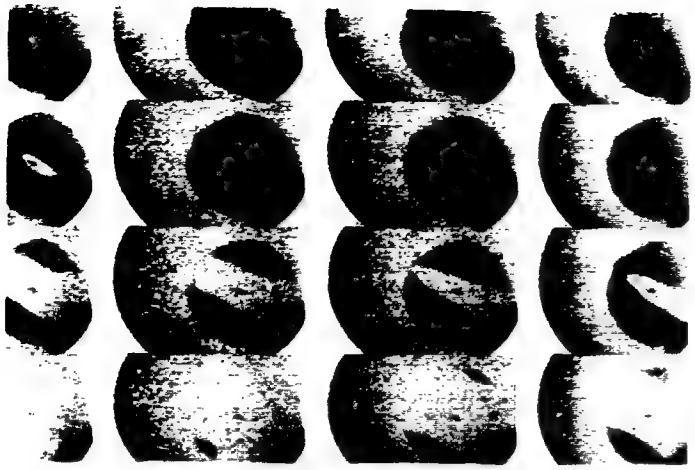

1

2

3

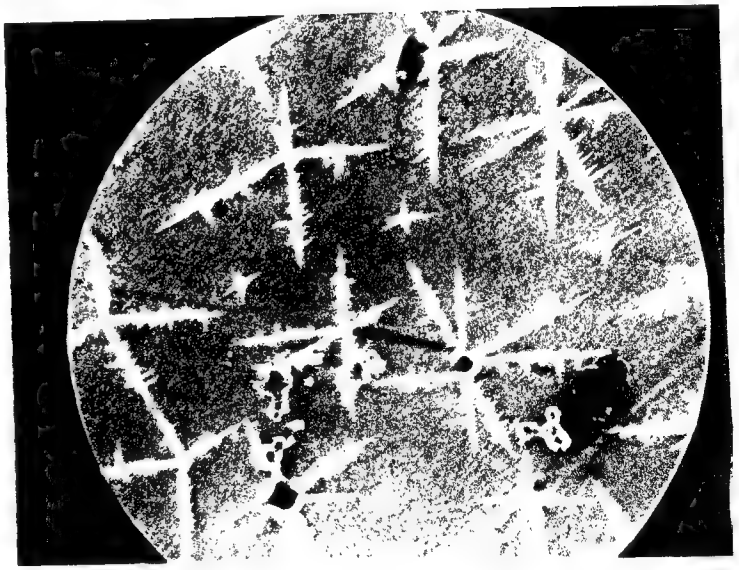

4

5

6

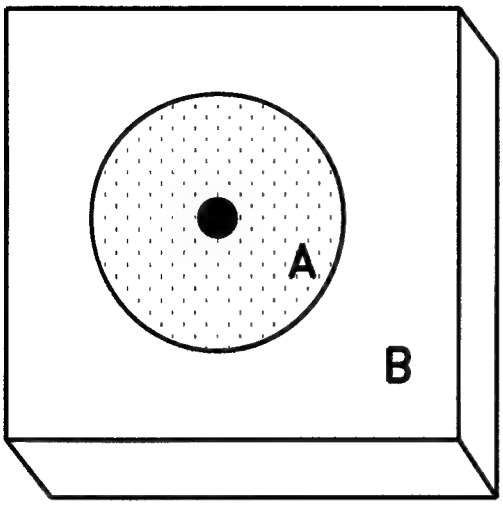
A
B

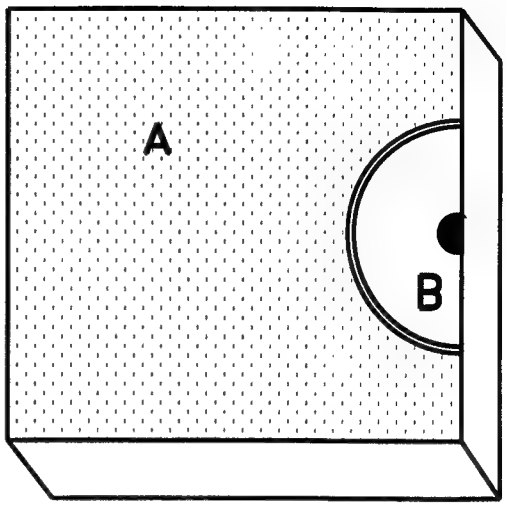
A
B

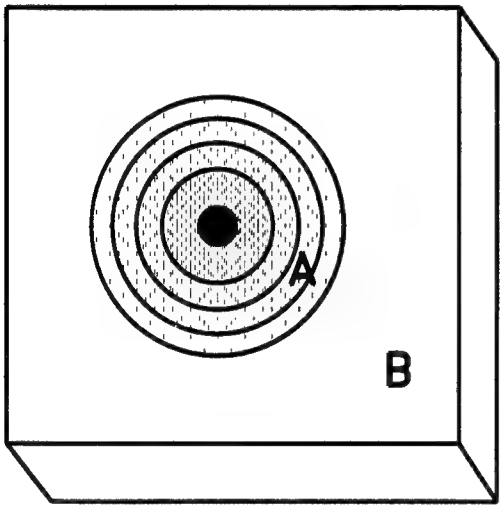
A
B

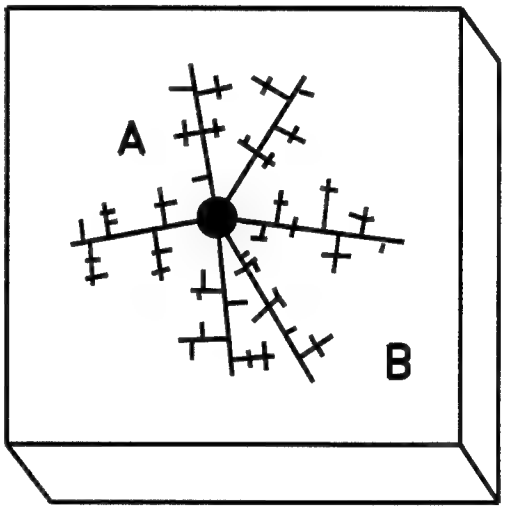
A
B

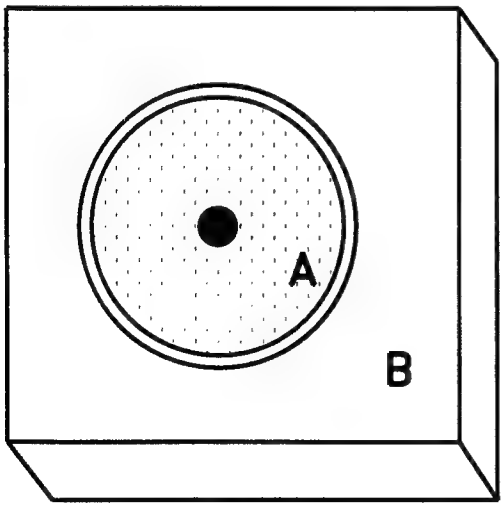
A
B

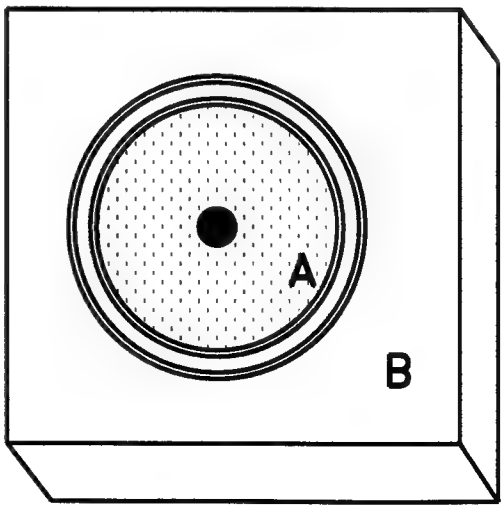
A
B

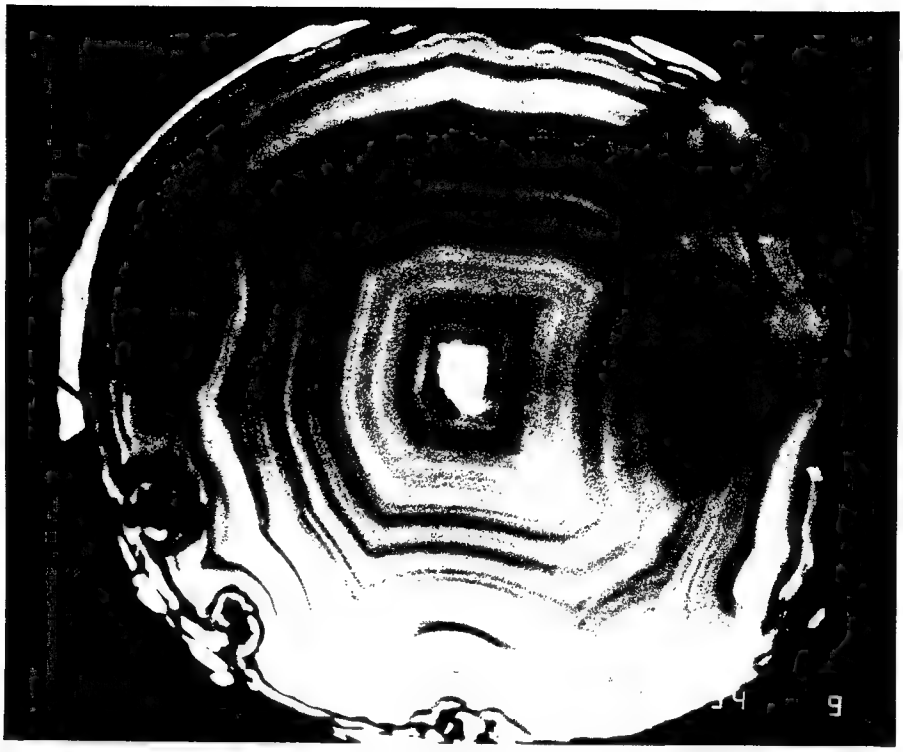

Fig 8

Synchrotron Radiation Photoelectron Emission Microscopy of Chemical Vapor Deposited and Natural Diamond Surfaces

J.D. Shovlin, M.E. Kordesch
Department of Physics
and the Condensed Matter and Surface Sciences Program
Ohio University, Athens, OH 45701,

D. Dunham, B.P. Tonner
Synchrotron Radiation Center and
University of Wisconsin Milwaukee, Milwaukee, WI 53211,

and

W. Engel
Fritz Haber Institute der Max Planck Gesellschaft
Faradayweg 4-6, Berlin, Germany, D-14195.

ABSTRACT

A variety of natural and chemical vapor deposited diamond surfaces have been imaged using a photoelectron emission microscope and synchrotron radiation in the 4-18 eV and 250-350 eV range. Both images and spatially resolved total electron yield curves were acquired simultaneously. Near-edge spectra at the carbon 1s edge show a resonance due to graphite; the image intensity varies uniformly in proportion to the C 1s edge intensity.

In the 4-18 eV range, no sharp features related to a photoemission threshold were observed below 7 eV in the electron yield curves on any of the specimens. The image contrast was not strongly dependant on the illumination energy. Natural type IIa diamond showed severe charging effects.

An applied electric field of 20 kV/cm was present during observation. No spectroscopic or image related evidence for field emission from the surfaces tested was found.

Introduction

A synchrotron-radiation based photoemission study of the boron doped diamond (111) surface by Himpsel, et al. [1] showed that this diamond surface possesses a negative electron affinity. The advent of chemical vapor deposited (CVD diamond), and doped CVD diamond, has stimulated interest in diamond for electronic devices, in particular for cold-cathode diamond electron emitters [2-8]. Photoemission measurements of the diamond surface using He resonance lamps and synchrotron radiation have also linked the electron emission properties of diamond to surface termination with hydrogen [9,10].

Several spectroscopic measurements have been made on diamond and CVD diamond using synchrotron radiation [10-15]. In this paper we present synchrotron radiation photoelectron emission microscopy (SR-PEEM) images for a variety of diamond surfaces, with micron-scale x-ray absorption near edge structure spectra (micro-XANES) for x-rays in the carbon K-edge energy range, and with vacuum ultra violet (VUV) photoyield curves for photons in the 4-18 eV range. Spatially resolved maps of electron emission from diamond surfaces may allow the identification of surface sites that are responsible for low field cold electron emission and possibly allow the correlation of the spectroscopic signature of negative electron affinity with features observed in an emission micrograph.

In particular, a sharp secondary electron emission peak in photoemission energy distribution curves is commonly observed

from various diamond surfaces that are regarded as "known negative electron affinity emitters" [1,9,10]. The peak occurs in the secondary electron emission spectra at a binding energy of about $h\nu - E_g$. In experiments to date $h\nu$ ranges from about 12 - 60 eV, and E_g is about 5.5 eV. For negative electron affinity diamond, electrons with a kinetic energy of Eg or higher will escape the surface.

The photoemission "electron distribution curve" methodology usually involves illumination at a fixed photon energy, while the emitted electrons are analyzed spectroscopically, with a relatively narrow energy window (< ~ 0.1 - 0.2 eV). This method is used even when the photon energy can be varied, as with synchrotron radiation. Another approach, used in core level spectroscopies (XANES, micro-XANES), involves collecting total electron yield curves as the incident photon energy from synchrotron radiation is varied using a monochrometer.

The SR-PEEM images collected from diamond surfaces reported here are a further variation on energy distribution curves and total yield curves. The PEEM microscope optics collect mostly secondary electrons. In the micro-XANES mode, the absorption edge jump (say at the C K-edge) also causes (low energy) secondary electron emission which predominates the electron signal used to form an image. The objective lens aperture acts as an energy selective element. However, even though a "total" yield measurement is made, sharp features are resolved in micro-XANES total yield curves (see for example fig 1, and ref.[19]).

In this paper PEEM images and total yield curves have been collected that extend the previous measurements to a range from $h\nu \approx E_g$ to E_{vac} and higher. At the approximate photon energy $h\nu \approx E_g$, the PEEM image would be formed from electrons emitted from negative electron affinity surfaces only, which could then be identified and located spatially in the image.

We have selected several "known low field cold electron emitters" from earlier measurements as well as natural single crystal diamond, so that they may be compared with "known negative electron affinity" surfaces. Pollycrystalline CVD diamond films should contain a variety of surface orientations and types, so that negative electron affinity emitters would show an emission threshold lower than those surfaces with positive electron affinity (about 7 eV). Image contrast in PEEM should then identify emission sites vs. incident photon energy.

Experimental:

The details of the emission microscope and data collection system have been described in ref. [19]. Briefly, the data acquisition system consists of the microscope optics, where electrons from the specimen are first accelerated through a potential difference of about 8 kV over 4 mm (or an accelerating field of 20 kV/cm). The electrons are collected, intensified and projected onto a channel plate assembly with a phosphor screen readout. The image on the phosphor screen is recorded outside of the vacuum chamber using a video camera, recorder and frame

grabber. The micro-XANES/VUV photoyield analysis is performed by selecting a specified number of pixels in the image for analysis using the frame grabber and software. Because the total electron yield curves for the VUV-yield images are a direct record of image intensity as a function of incident photon energy, no ratio or relative yield methods commonly used to eliminate structure in electron yield curves due to the transmission function of the monochrometer were applied.

The x-ray spectra and images were acquired using the 10 m Toroidal Grating Monochromator (TGM) beamline, the low energy yield curves and images were acquired using the Aluminum Seya-Namioka (Al SEYA) beamline, both at the Synchrotron Radiation Center at Stoughton, WI.

A boron-doped CVD diamond on a silicon substrate was observed at the carbon K-edge on the 10 m TGM. Several specimens were examined on the Al SEYA: both natural diamond (IIa and IIb: Doubbledee Harris Diamond Corp., Mount Arlington, NJ) and [100] textured microwave plasma CVD (MPCVD) films with an overlayer of sputter-deposited gold, gold coated and uncoated CVD diamond (Hot filament assisted, HFCVD), amorphic diamond (a tradename for laser ablated diamond), CVD and natural diamond field emitter arrays, and graphite tape as a control specimen.

No image related or spectroscopic differences were observed between CVD diamond "as grown" and washed in a chromic acid-sulfuric acid solution [20]. All specimens were rinsed in isopropanol to remove contaminants [21]. The specimens were

mounted on a transfer stub of aluminum using graphite adhesive tape. The transfer stub could not be heated; all spectra were acquired at 300 K (room temperature).

In order to examine the contribution of second order light from the Al Seya-Namioka monochrometer to the electron yield curves, the isolation valve separating the PEEM chamber from the beamline was closed. This valve is fitted with a sapphire window that allows low energy radiation to pass through the window while the valve is in the closed position. The window is uv grade sapphire, 2mm thick, and will allow about 40% light transmission at 7 eV and a steep cutoff at energies above this value.

Results:

A boron-doped CVD diamond surface imaged using the 10m TGM is shown in figure 1 a). The image data is collected on videotape, so that a continuous record of the image and image contrast as a function of incident photon energy is available. Figure 1 a) was photographed from the monitor at an energy above the C K-edge. Figure 1 b) shows several micro-XANES spectra for a single crystallite in the film (top curve is for the rectangular crystal marked with an arrow in 1 a)), and areas with smaller, unresolved crystal structures (bottom curves). It is clear from the total yield curves that sharp features, such as the peak at ~ 285 eV, can be resolved in the secondary electron yield.

Figure 2 a) is a typical image from an unbacked, [100]

textured MPCVD diamond film. The illumination in this image is the zero order light from the Al SEYA. The micrograph in figure 2 b) was taken from the exact same sample and location, but at an incident photon energy of 15 eV; an energy that corresponds to the maximum intensity on the Al SEYA (with the lowest range grating). Figure 2 c) is a micrograph taken with zero order light of a diamond emitter array fabricated by diamond CVD on a silicon substrate [8]. The SR-PEEM image in figure 2 d) shows a diamond array consisting of 100 μm diameter natural diamond octahedra imbedded in a copper matrix, with CVD diamond grown on the tips of the pyramids. These arrays are described by Angus and Geis in ref. [3]. Only the copper matrix between the diamonds, and the small CVD diamond at the tips of the pyramids are bright in the image.

In figure 3, a)-f), VUV photoyield spectra collected from small, selected sample areas are displayed for photon energies from about 4 eV to 9 eV. The specimens measured are a) boron-doped type IIb natural diamond (random orientation), b) natural type IIa diamond (100), c) graphite tape, d) "amorphic" diamond, e) [100] textured MPCVD diamond, f) same as e) covered with 15 nm sputtered gold.

Figure 4 a) shows a yield curve from a boron-doped MPCVD diamond on silicon, 4 b) is the same as a) but with the valve to the beamline closed, so that the sample was illuminated through a sapphire window to exclude second order radiation from the monochrometer grating. The transmission function for the window

is drawn in figure 4. The dashed curve shows percent transmission for first order light.

The "grating horizon", the photon energy at which the first photons pass through the monochrometer-slit assembly and reach the sample, is calculated to be about 4.07 eV.

Discussion:

The micro-XANES spectra are comparable to large-area near edge spectra which have been dealt with extensively in previous work [10-15] and in electron energy loss near edge spectra [16-18]. The peak at 285 eV corresponds to the 1s to π^* excitation characteristic of sp^2 bonds in graphitic carbon. The steep intensity rise at 289 eV is due to C1s to σ^* transitions.

The oscillations beyond the near edge structure (> 298 eV) are the equivalent of extended x-ray absorption fine structure spectra and, and can be used to determine the local geometry and coordination of carbon in the film. The peak at about 328 eV is particularly characteristic of diamond [16-18].

No spatially resolved material contrast was observed in this micrograph (fig. 1 a)), although a distinct overall reduction in intensity was observed between the sharp near-edge feature at 285 eV and the edge-jump at 298 eV and above. The image contrast in this micrograph is due mostly to topography [22]. The orientation of each crystallite relative to the microscope axis determines what fraction of the emitted electrons are collected by the objective lens, so that crystallites oriented with their

surface normals exactly co-linear with the optical axis of the microscope will be the brightest in the image. On the scale of this measurement, the difference between the top curve and the bottom two is therefore only due to allignment of the crystallite faces relative to the microscope optical axis. It would be possible to turn the specimen in such a way that the dark areas in the image become bright due to better allignment, while the intensity from previously aligned crystallites diminishes. The "orientation" or "aperture" effect of crystallite alignment with the microscope axis has by far the largest effect on image intensity. In a polycrystalline film, we expect that more subtle compositional effects are masked by the intensity variations due to the distribution in crystallite orientation relative to the optical axis.

With the exception of natural type IIa diamond, which charged during examination, all of the diamond specimens gave excellent PEEM images at low illumination energy (4-18 eV). There were no spatially resolved variations in photoyield as a function of illumination energy in any of the images. The yield curves in figure 3 show no obvious emission threshold, contrary to what might be expected for natural diamond with a band gap of over 5 eV. No sharp change in electron emission was observed for any of the specimens, in particular for the natural diamonds between 4 and 6 eV.

Several of the diamond specimens tested have shown low field cold electron emission at slightly higher applied fields, in

particular the HFCVD and MPCVD films [5], the CVD diamond array [8], and the gold coated [100] textured MPCVD film [4]. The test conditions in an emission microscope are ideally suited to field emission studies, since the accelerating electric field is part of the imaging system. If any of the specimens were low field cold emitters, or negative electron affinity emitters, some areas of the film might be expected to show an emission threshold signature in the VUV photoyield curves, that could be correlated with changes in the image. The total yield curves in figure 3, however, show no features due to a negative electron affinity, no features due to a photoemission threshold, or any sharp features at all.

The curve in figure 4b does show a "threshold-like" intensity variation at about 7eV; E_{vac} for natural diamond. The transmission of light through the window decreases with increasing photon energy, so that, ideally, about 40% transmission is achieved at 7eV. The intensity ratio at 7eV, and more significantly, at energies where the transmission of light through the window should be substantially higher, does not correspond to the observed reduction in count rate (absolute count rates are between a factor of 10 and 100 less than expected due to window transmission cutoff below 7 eV). We therefore conclude that a significant portion of the intensity observed in the curves in figure 3 is due to second order light. Within the limits of this data, we can report only that no threshold or sharp feature was observed in the measured range between 4 and

7eV. The curve in figure 4 b) was acquired with approximately 12 times longer acquisition times relative to 4 a) and are plotted on the same scale.

Summary:

Several different diamond surfaces have been imaged using an emission microscope and synchrotron radiation in the 4-18 eV and carbon K edge energy range. Lateral variations in electron yield were not resolved over this range that could be identified with spectral features in micro-XANES spectra or VUV total electron yield curves.

Heating the specimens and exposing them to atomic hydrogen to produce a H terminated surface [1,9,10] may be necessary to observe effects due to negative electron affinity in either the VUV photoyield spectra or the photoelectron emission micrographs.

A further refinement of the present experiment would be the use of an energy filtering PEEM, such as the paraxial ray imaging spectromicroscope [21], and/or a normal incidence monochrometer with less second order light transmission in the desired range.

Acknowledgements:

This work was supported by the Ballistic Missile Defense Organization through the Office of Naval Research Grant No. N00014-91-J-1596. W.Engel, J.Shovlin and M.Kordesch acknowledge travel support from NATO. The Synchrotron Radiation Center at

Stoughton, WI is supported by the Department of Energy. We would like to thank M. Geis, K. Jamison, A. Kirkpatrick and E. Sevilliano for providing several diamond samples.

References:

{shovlin,kordesch}@helios.phy.ohiou.edu, dunham@csd.uwm.edu, tonner@src.wisc.edu, engel@fhi-berlin.mpg.de

1. F. J. Himpsel, J.A. Knapp, J.A. van Vechten, and D.E. Eastman, Phys. Rev. B, 20, 624 (1979).
2. M.W. Geis, N.N. Efremow, J.D. Woodhouse, M.D. McAleese, M. Marchywka, D.G. Socker and J.F. Hochedez, IEEE Elec.Dev.Lett., 12, 456 (1991).
3. J. Angus and M. Geis, Scientific American, October 1992, pg. 84.
4. J.D. Shovlin and M.E. Kordesch, Appl. Phys. Lett., 65, 863 (1994).
5. C. Wang, A. Garcia, D. Ingram, M. Lake and M.E. Kordesch, Electronics Lett., 27, 1459 (1991).
6. N.S. Xu, R.V. Latham and Y. Tzeng, Electronics Lett., 29 1596 (1993).
7. N.S. Xu, Y. Tzeng and R.V. Latham, J.Phys.D: Appl. Phys., 26 1776 (1993).
8. M.E. Kordesch, in Proc. 3rd Intl. Symp. Diamond and Diamond Materials, J.P. Dismukes and R.K. Ravi, eds., Proceedings Vol. 93-17, The Electrochemical Society, Pennington NJ, (1993) 787-793.

9. J. Van der Weide and R.J. Nemanich, Appl.Phys.Lett., 62 1878 (1993).

10. B.B. Pate, Surf. Sci. 165, 83 (1986).

11. J.K. Simons, R.V. Dueval, S.P. Frigo, J.W. Taylor and R.A. Rosenberg, J. Appl. Phys., to be published.

12. J. Nithianandam, J.C. Rife and H. Windischman, Appl. Phys. Lett. 60, 135 (1992).

13. G. Comelli, J. Stohr, W. Jark and B.B. Pate, Phys.Rev. B, 37, 4383 (1988).

14. J.F. Morar, F.J. Himpsel, G. Hollinger, J.L. Jordan, G. Huges and F.R. McFeely, Phys. Rev. B, 33, 1340 (1986).

15. B. Pate, I. Lindau and W.E. Spicer, Proc. 17th Intern. Conf. Phys. Semicond., J.D. Chadi, W.A. Harrison, eds. pg. 1181, Springer-Verlag, New York (1985).

16. H.K. Schmidt, in Proceedings of the 13th International Congress on Electron Microscopy, B. Jouffrey and C Colliex, eds., Vol. 1, Les Editions de Physique, France, pg. 695.

17. S.D. Berger, J. Bruley, L.M. Brown and D.R. McKenzie, Ultramicroscopy 28, 43 (1989).

18. S.D. Berger, D.R. McKenzie and P.J. Martin, Phil. Mag. 57, 285 (1988).

19. B.P. Tonner, G.R. Harp, S.F. Koranda and J. Zhang, Rev. Sci. Instrum. 63, 564 (1992).

20. R.E. Thomas, R.A. Rudder, R.J. Markunas, D. Huang and M. Frenkelach, J. Chem. Vapor Depos. 1, 6 (19920

21. W. Engel, D.C. Ingram, J.C. Keay and M.E. Kordesch, Diamond

Relat. Mater., 3, 1227 (1994).

22. G.F. Rempfer, K.K. Nadakavukaren and O.H. Griffiths, Ultramicroscopy 5, 437 (1980).

23. B.P. Tonner, Nucl. Instr. and Meth. A291, 60 (1990).

Figure Captions:

1. a) SR-PEEM image of a boron doped CVD diamond above the C K-edge. The arrow marks the crystallite from which the spectra in 1 b) are taken. The crystallite is about 10 μm on an edge.

   b) Micro-XANES spectra from the crystallite in figure 1 a), top curve, the lower curves are from dark areas near the crystallite.

2. a) SR-PEEM micrograph of [100] textured, unbacked MPCVD diamond film using zero order light from the Al SEYA.

   b) Same as a) at 15 eV. Note the light disks in the centers of the (100) faces, due to deflection of electrons out of the collection aperture of the objective lens due to high fields at the crystallite edges. The (100) faces are about 10 μm on an edge.

   c) SR-PEEM micrograph of diamond field-emitter array using zero-order light. Fabricated by diamond CVD on silicon [10]. Diamond spacing is 20μm.

   d) SR-PEEM micrograph of diamond array. Array consists of 100μm diameter natural diamond octahedra imbedded in a copper matrix with CVD diamond grown on the pyramidal tips. [6]. Due to aperture effects, only the copper matrix between the pyramids, and the CVD diamond at the tips, are bright in the image.

3. VUV Micro-photyield spectra of A) IIb natural diamond, B) IIa natural diamond, C) graphite tape, D) amorphic (laser

ablated) diamond, E) Au coated [100] MPCVD diamond, F) [100] MPCVD diamond, pictured in figure 2 a) and b).

4. VUV Micro-photoyield spectra of A) boron-doped MPCVD diamond film on silicon, B) same as A), with beamline valve closed, and a sapphire window in the beampath. The relative intensity of A) to B) on the basis of acquisition time is B)= 12xA), i.e. B) is about 12 times less intense relative to A).

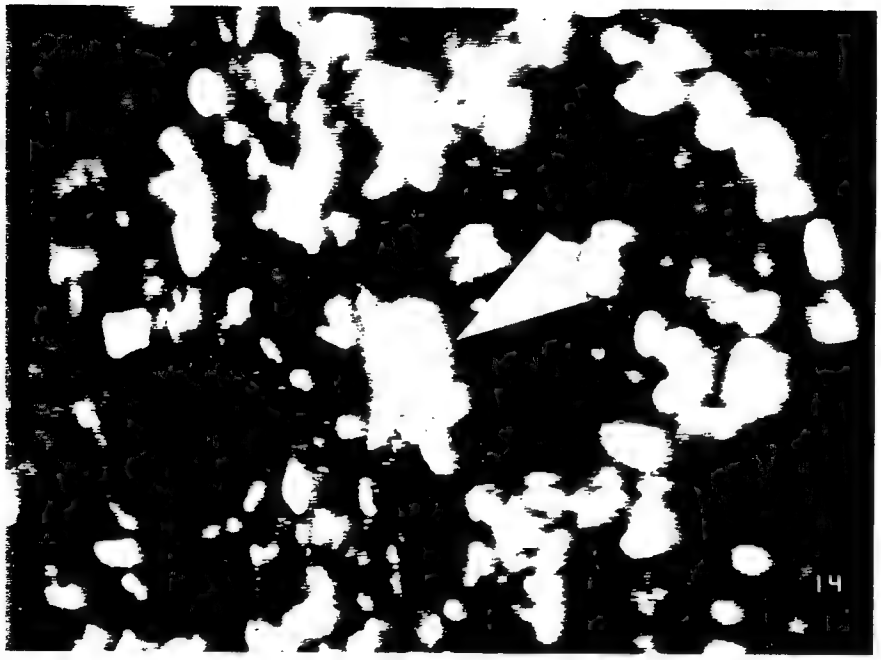

Fig. 1 (A)

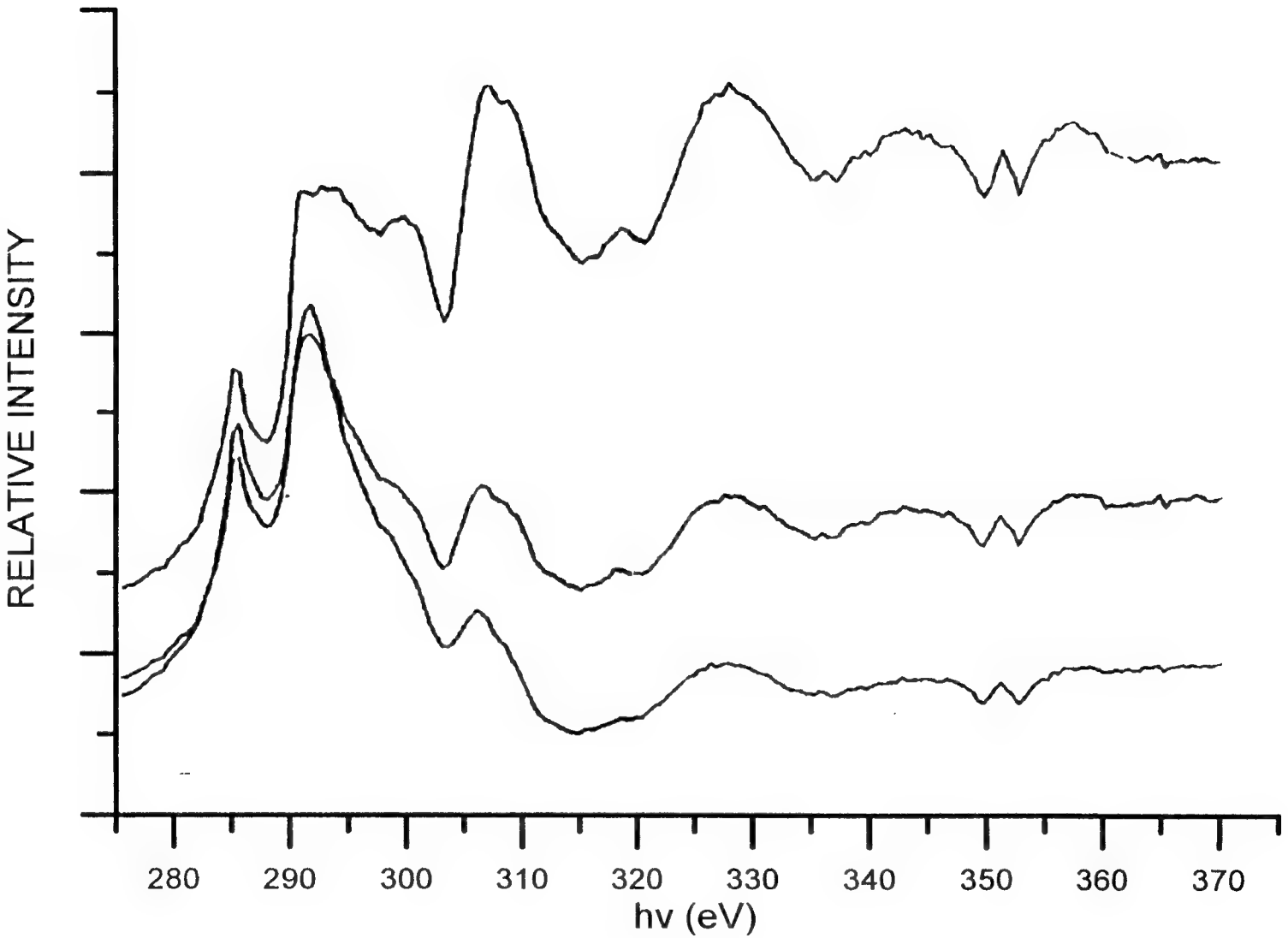
RELATIVE INTENSITY
280
290
300
310
320
330
340
350
360
370
hv (eV)

Fig. 1 (B)

(A)

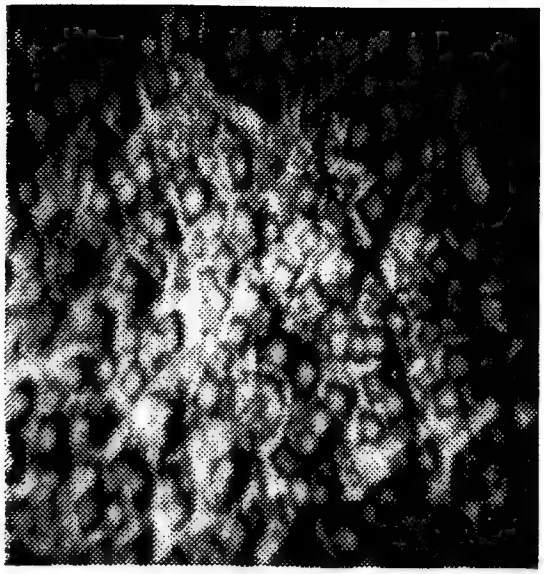

(B)

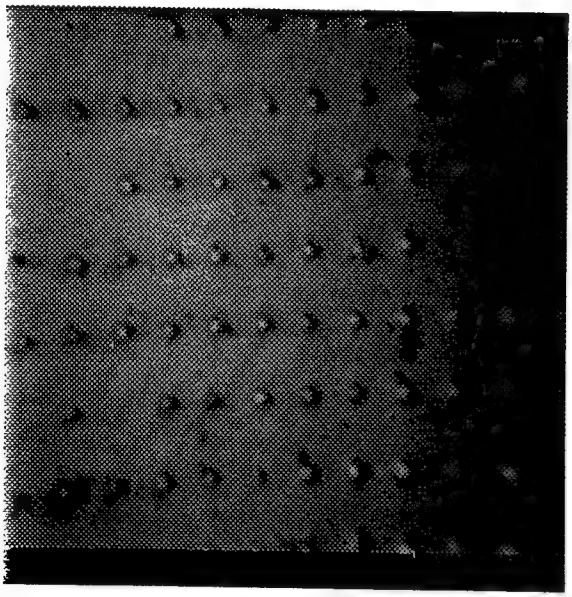

(C)

(D)

Fig. 2

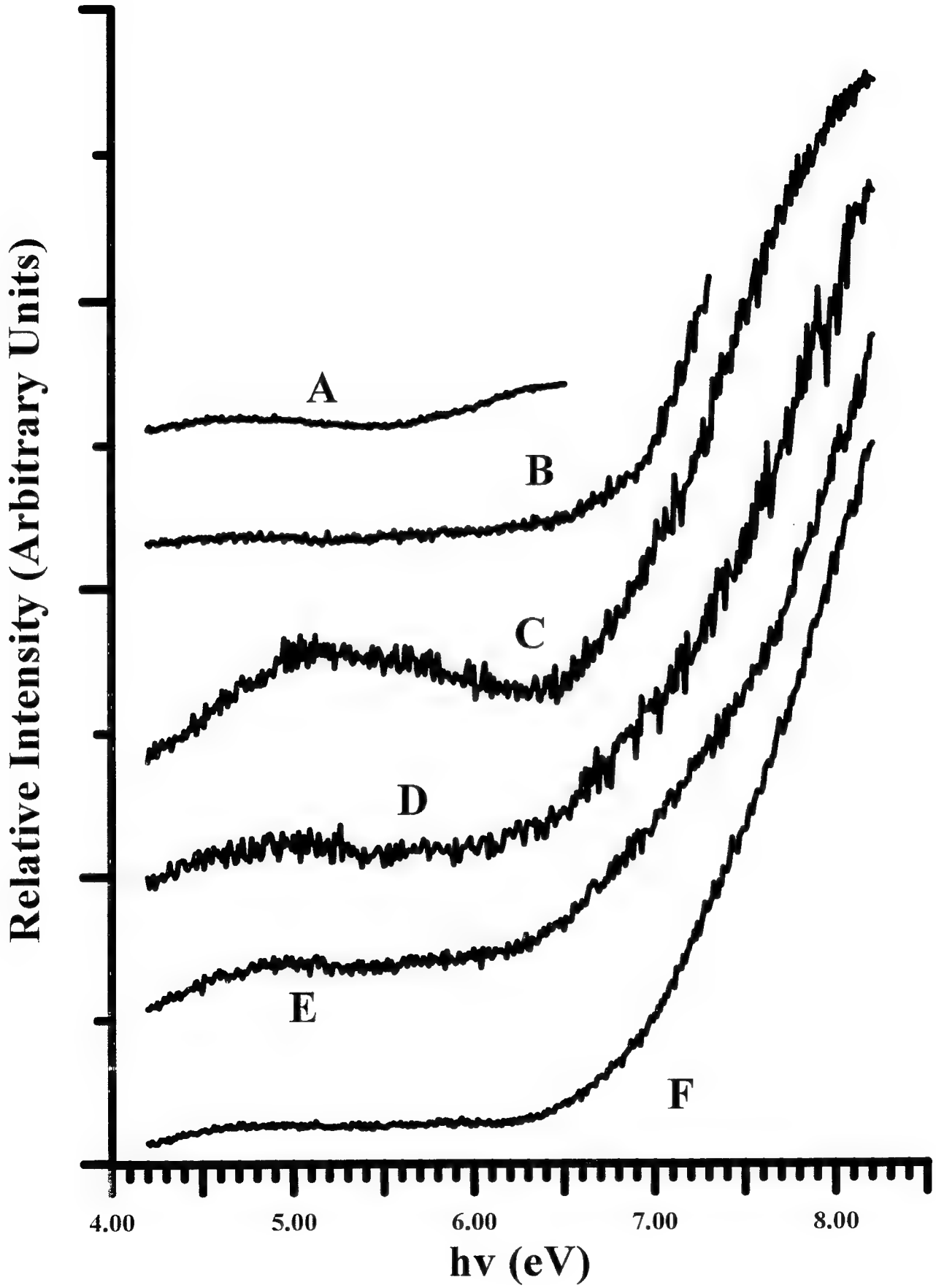
Relative Intensity (Arbitrary Units)
A
B
C
D
E
F
4.00
5.00
6.00
7.00
8.00
hv (eV)

Fig. 3

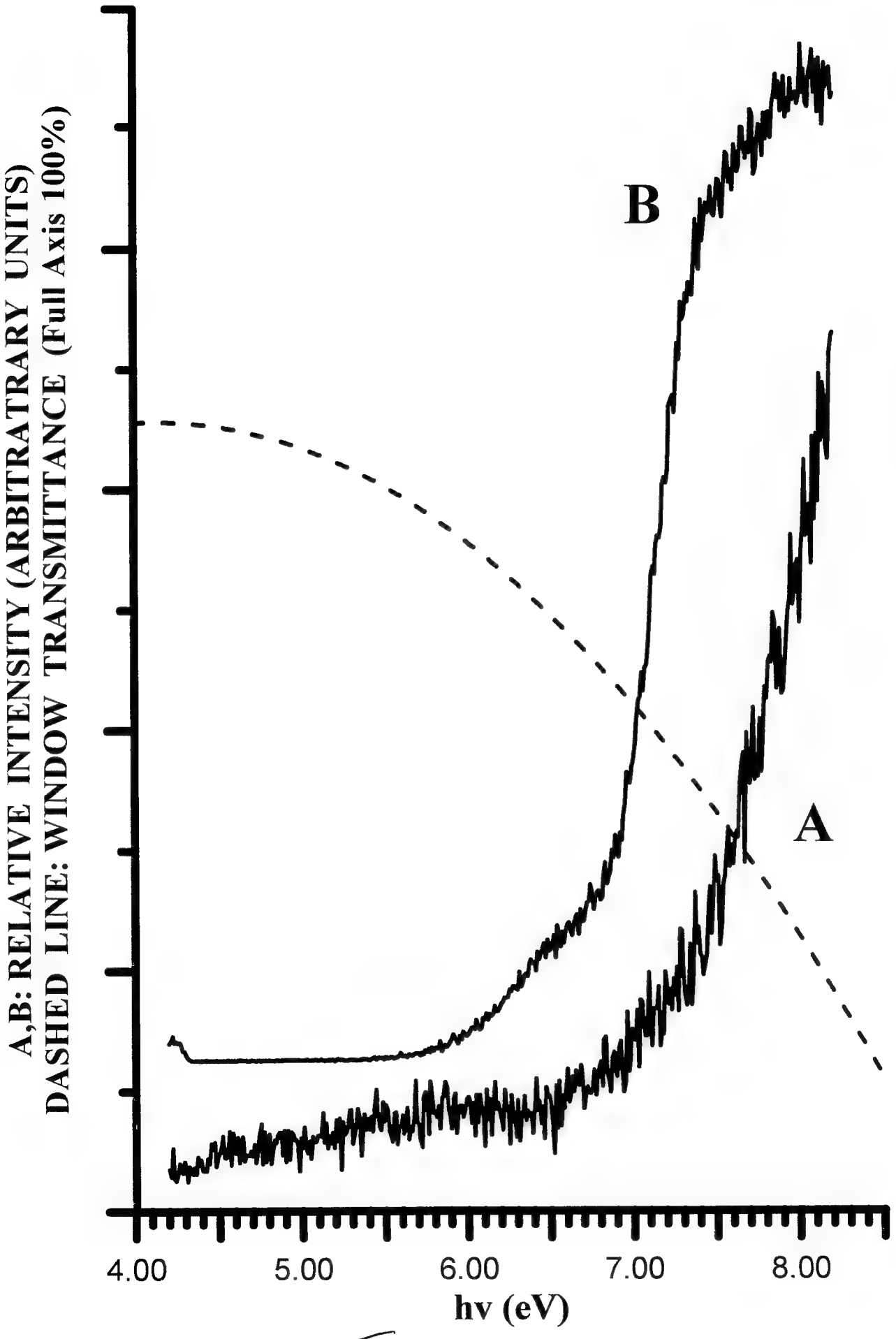
A,B: RELATIVE INTENSITY (ARBITRATRARY UNITS)
DASHED LINE: WINDOW TRANSMITTANCE (Full Axis 100%)
B
A
4.00
5.00
6.00
7.00
8.00
hv (eV)

Fig. 4

TWO-DIMENSIONAL GROWTH-FRONTS OBSERVED ON MOLYBDENUM SURFACES

A dissertation presented to

The Faculty of

The College of Arts and Sciences of Ohio University

In partial fulfillment

of the requirements for the degree

Doctor of Philosophy

Adrian Luis Garcia

August 1994

Garcia. Adrian Luis. Ph.D. August 1994. Physics

Two–Dimensional Growth–Fronts Observed on Molybdenum Surfaces

(140 pp.)

Director of Dissertation: Dr. Martin E. Kordesch

The purpose of the research presented in this dissertation is to study in *real–time* the nucleation and growth of carbon overlayers on Mo(100) and Mo(310) as a first step towards hetero–epitaxial growth of diamond films.

Prior to the carbon deposition, the clean Mo surface at 700–1000 K was saturated with oxygen. A 5%CH_4/H_2 gas mixture passed over a hot filament was blown onto the oxygen covered surface. The 5%CH_4/H_2 was admitted into the chamber until a pressure of 1×10^{-6} Torr was reached.

On the oxygen saturated surface *lateral growth* of an *ordered overlayer* was observed in real–time with the *photoelectron emission microscope*. The lateral growth proceeded as a reaction front traveling across the crystal in a *wave–like* fashion. A *reaction area* in the form of a band running parallel to the reaction front was observed on both Mo(100) and Mo(310). Oxygen was removed at the leading edge of the reaction area, and carbon was deposited. With the O/Mo(100) substrate at 1300 K, the reaction front had a speed in the range 0.2–2 μm/s. A (5×1) array of (2×1) domains was obtained for the overlayer grown on Mo(100).

Two kinds of growth were observed during the deposition experiments on Mo(310): *two-dimensional growth* like the one observed on Mo(100), and *island growth* around nucleation centers. With the substrate at 950 K, the reaction area observed during deposition was divided into *four bands*. Prior to carbon deposition, point Auger analysis of the Mo(310) surface showed the MNV transitions of Mo (183 and 218 eV), and the KLL transitions of oxygen (508 eV) and carbon (266 eV). After the deposition a new peak was observed at 147 eV corresponding to the LMM transition of sulfur. Scanning Auger analysis showed a boundary separating the carbon/sulfur and oxygen

covered areas.

Both the behavior and visual aspect of the reaction fronts, as well as the onset of the reaction, depend on the substrate temperature. On Mo(100) at 1300 K, the reaction front has the appearance of a uniform band of growing width with the leading edge moving toward the oxygen covered region while the back end remains stationary. On Mo(310) at 950 K, the reaction area shows a multi-band structure whose existence has been attributed to the combination of two on-going processes taking place at the film-substrate interface: surface diffusion of atomic species adsorbed in the reaction area, and segregation of sulfur from the bulk. A model of these processes is presented.

Approved Martin E. Underhill
Associate Professor of Physics

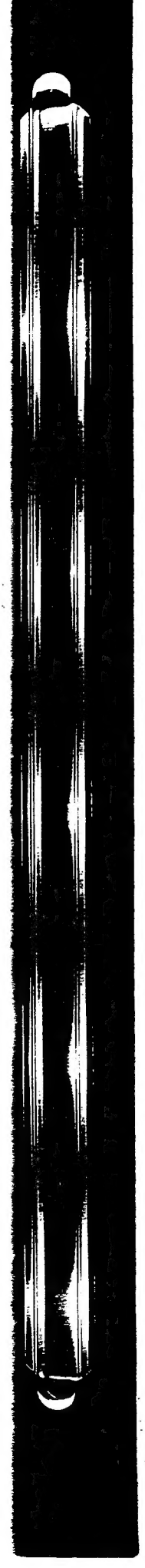

An Electron Microscope to Monitor the Melting of Metals

A Thesis

Presented to

The Honors Tutorial College

Ohio University

In Partial Fulfillment

of the Requirements for Graduation

from the Honors Tutorial College

with the degree of

Bachelor of Science in Physics

---

by

Stephen Louis Pellathy

June 1994